Applying Machine Learning to Characterize and Transport the Relationship Between Seismic Structure and Surface Heat Flux

Shane Zhang[*1] and *Michael H. Ritzwoller*[1]

[1] Department of Physics, University of Colorado Boulder, Boulder, CO 80309, USA.

Abstract

Geothermal heat flux beneath the Greenland and Antarctic ice sheets is an important boundary condition for ice sheet dynamics. Subglacial heat flux is rarely measured directly, so it has been inferred indirectly from proxies (e.g. seismic structure, magnetic Curie depth, surface topography). We seek to improve understanding of the relationship between heat flux and one such proxy—seismic structure—and determine how well heat flux data can be predicted from the structure (the *characterization* problem). We also seek to quantify the extent to which this relationship can be transported from one continent to another (the *transportability* problem). To address these problems, we use direct heat flux observations and new seismic structural information in the contiguous US and Europe, and construct three Machine Learning models of the relationship across a hierarchy of model complexity (Linear Regression, Decision Tree, Random Forest). The more complex models fit smaller scale variations in heat flux. We compare the models in terms of model interpretability, accuracy to predict heat flux, and transportability from one continent to another. To evaluate model accuracy, we divide data on the same continent into training and validation datasets, and then validate

[*]shane.zhang@colorado.edu

the model (trained from the training data) with validation data. We measure model transportability by cross-validating the US-trained models against European heat flux, and vice versa. We find that the Random Forest and Decision Tree models are the most accurate, while the Linear Regression and Decision Tree models are the most transportable. The Decision Tree model can uniquely illuminate the regional variations of the relationship between heat flux and seismic structure. From the Decision Tree model, uppermost mantle shear wavespeed, crustal shear wavespeed and Moho depth together explain about half of the observed heat flux variations in both the US ($r^2 \approx 0.6$ (coefficient of determination), RMSE $\approx 8\,\mathrm{mW/m^2}$ (Root Mean Squared Error)) and Europe ($r^2 \approx 0.5, \mathrm{RMSE} \approx 13\,\mathrm{mW/m^2}$). Uppermost mantle wavespeed is a much stronger predictor than the other two variables combined. Transporting the US-trained models to Europe reveals that the geographical distribution of heat flux can be reasonably predicted ($\rho = 0.48$ (correlation coefficient)), but the absolute amplitude of the variations cannot ($r^2 = 0.17$), similarly from Europe to the US ($\rho = 0.66, r^2 = 0.24$). We attribute the transportability deterioration to differences between the continents in seismic structural imaging data and parameterization, and crustal radiogenic heat production. Despite these issues, our method has the potential to improve the reliability and resolution of heat flux inferences across Antarctica. Furthermore, our validation and cross-validation methods can be applied to heat flux proxies other than seismic structure, which may help resolve inconsistencies between existing subglacial heat flux inferences using different proxies.

Key words: Heat flow; Seismic tomography; Machine Learning; Heat generation and transport; Glaciology; Antarctica

Section: Heat flow and volcanology

Short title: Relating seismic structure with heat flux

Contents

List of Figures

1 Introduction

1.1 Geothermal heat flux

Surface geothermal heat flux represents the rate of heat loss from the solid Earth. Heat flux holds clues for deciphering the thermal evolution within the Earth [1], can inform the exploration for geothermal energy [2], and affects the thermal state of various cryospheric realms, such as permafrost [3] and continental ice sheets [4–8].

1.2 Motivation

In particular, heat flux can influence the lower boundary conditions of ice sheets, notably the state of freezing to the subglacial bed and the melt extent which can strongly affect ice flow. However, direct observations of heat flux beneath the Greenland and Antarctic ice sheets remain rare because of the difficulty and expense of drilling to the base of the ice sheet. Thus, heat flux beneath the Greenland and Antarctic ice sheets imposes a major uncertainty in ice sheet models that aim to predict future melting and sea level changes [8]. Therefore, indirect inferences of heat flux beneath the Greenland [9–17] and Antarctic ice sheets [9, 18–30] have attracted much recent interest.

In both Greenland [17] and Antarctica [31], inferences of heat flux are largely made through different sets of proxies. These inferences have not yet converged to produce a consistent model of heat flux beneath the major ice sheets. The proxies include seismic structure [9, 24], magnetic Curie depth [18, 21], and surface topography [29]. More importantly, many studies that infer heat flux have not yet been subject to validation in which the predicted values are compared with ground truth or observations not included in making the prediction. Such validation is crucial to the evaluation of the transportability of inference methods from the region where they are developed (where heat flux measurements may be plentiful) to other regions (where heat flux observations are scarce or absent entirely, such as Greenland

and Antarctica).

We investigate the ability to predict surface heat flux using seismic structure as a proxy. We use data from the contiguous US and Europe (**section 2**) because most of the world's continental heat flux observations are obtained there [32] and high-resolution regional seismic structure has been imaged recently [33, 34]. We focus on seismic structure as a proxy because seismic tomography provides information at depth, with images of both the crust and mantle, and can thus attribute effects on heat flux to specific depths. Many other proxies cannot do this.

1.3 Problem statement

The urgency of estimating geothermal heat flux beneath polar ice sheets and the inconsistencies between existing estimates motivate the two main questions we pose in this study.

First, what is the relationship between seismic structure and surface heat flux in a given region? Specifically, how well is heat flux predicted by seismic structure, which seismic structural variable(s) is most predictive of heat flux, and how is the relationship specified? We refer to this problem as the *characterization* problem.

Second, how well can the relationship between seismic structure and surface heat flux be transported from one continental setting to another? In particular, what aspects of the relationship are similar or dissimiliar between various continents and what causes the dissimiliarity? We call this problem the *transportability* problem.

To be precise, let r_i stand for a location on the Earth's surface, and $\hat{q}(r_i)$ for heat flux to be predicted at location r_i, and $v(z, r_i)$ for 1-D local seismic structure as a function of depth z beneath location r_i, and $q^{\text{obs}}(\{r_j\}_{j=1}^{N_{\text{obs}}})$ for a total of N_{obs} heat flux observations at locations $\{r_j, j = 1, 2, \ldots, N_{\text{obs}}\}$ and $w(\{r_j\}_{j=1}^{N_{\text{obs}}})$ for their associated weights (uncertainties). We define the relationship between heat flux and seismic structure as a Machine Learning model $\hat{f}$ that predicts heat flux $\hat{q}(r_i)$ based on seismic structure $v(z, r_i)$, and heat flux observations

$q^{\text{obs}}(\{r_j\}_{j=1}^{N_{\text{obs}}})$ with associated weights $w(\{r_j\}_{j=1}^{N_{\text{obs}}})$,

$$\hat{q}_i = \hat{f}(v_i, q^{\text{obs}}, w; \Theta). \tag{1}$$

Here, Θ denotes parameters in the model, and to avoid cluttering, $\hat{q}_i \equiv \hat{q}(r_i)$, $v_i \equiv v(z, r_i)$, $q^{\text{obs}} \equiv q^{\text{obs}}(\{r_j\}_{j=1}^{N_{\text{obs}}}), w \equiv w(\{r_j\}_{j=1}^{N_{\text{obs}}})$.

1.4 Methodology

We describe here two particular methodological approaches used to address aspects of both the characterization and transportability problems.

Our first approach focuses on understanding the relationship using Machine Learning models across a hierarchy of complexity. In the characterization problem, we seek to specify how a specific prediction of heat flux, $\hat{q}$, is made from the model $\hat{f}$. We achieve this by comparing three Machine Learning models $\hat{f}$ across a hierarchy of complexity, namely the Linear Regression model, the Decision Tree model, and the Random Forest model. These models model the relationship across continental, regional, and local scales, respectively (**section 3**). This is also essential for the transportability problem, where we seek to understand how the relationship differs between different continents.

Our second approach focuses on holding out certain data to evaluate a specific aspect of a model (**section 3.2**). In the characterization problem, we are interested in how well heat flux can be predicted by seismic structure in a given region. Therefore, for both the US and Europe, we divide heat flux observations into two disjoint subsets of data: the training and validation datasets. In both continents, we use the training data to train the model, and then validate the trained model on the validation data (**section 4.1**). We refer to this procedure as *validation*. In the transportability problem, we are interested in how well can the relationship be transported from one continental setting to another. Hence, we take models trained in the US and then apply them to Europe, and vice versa (**section 4.2**). We

call this process as *cross-validation*. Both validation and cross-validation are important tests of a model to predict heat flux.

1.5 Outline

We summarize this methodology to tackle the characterization and transportability problems in **Fig. 1**. We begin by describing the data sources and quality control of heat flux data and seismic data used in this study (**section 2**). Second, we introduce the three Machine Learning models (Linear Regression, Decision Tree, and Random Forest) which we use to investigate the relationship between heat flux and seismic structure (**section 3**). We then present the validation results made in each of the continents, the contiguous US and Europe, and the cross-validation results by applying a model determined on one continent to data from the other continent (**section 4**). Finally, we discuss the limitations of this work and the potential applications to polar regions and other continents (**section 5**).

1.6 Notation

We use geothermal heat *flux* to refer to the amount of heat per unit time per unit area ($\mathrm{J}/(\mathrm{s}\cdot\mathrm{m}^2)$) transported from the Earth's interior to surface. Heat *flow* is also commonly used in the literature to refer to the same quantity, but we do not use this term.

We use a hat (as in $\hat{q}$) and a superscript "obs" (as in q^{obs}) to denote predicted and observed quantities, respectively (e.g. **eq.** (1)).

Each Machine Learning model $\hat{f}$, along with model parameters Θ, specifies a relationship between heat flux and seismic structure. Thus we use the words *model* and *relationship* synonymously.

The seismic structure, $v(z, r)$, is inferred from seismic inversions, the results of which are often referred to as seismic tomography *models*. We refer to $v(z, r)$ as seismic *structure* or structural *information* or structural *variables* to avoid confusion with the Machine Learning *models*, $\hat{f}$. Therefore, here, a model specifies the relationship between seismic structure and

heat flux.

Here we use *validation* to mean the splitting of training and validation data on the same continent, which evaluates model *accuracy*. In contrast, we use *cross-validation* to denote transporting models trained from one continent to the other, which assesses model *transportability*. In the Machine Learning literature, the *cross-validation* procedure is often used to mean our *validation*; sometimes the data are split into training, validation, and *test* data, where the test data are used in a process somewhat similar to our *cross-validation*.

2 Data

In this section, we first discuss the data sources for heat flux observations, and focus on quality control (**section 2.1**). We then discuss seismic structural variables, aiming to extract those most predictive for heat flux (**section 2.2**).

We often use MAD (Median Absolute Deviation) as a robust measure of the variability of any variable $x_k, k = 1, 2, 3 \ldots,$

$$\mathrm{MAD}(x) \equiv \alpha \,\mathrm{Median}\left(|x_k - \tilde{x}|\right), \tag{2}$$

where $\tilde{x} \equiv \mathrm{Median}(x), \alpha \approx 1.5$ such that the MAD of a Gaussian distribution is the same as its standard deviation. Therefore, MAD is similar to standard deviation but less prone to outliers.

2.1 Geothermal heat flux

2.1.1 Data Sources

Our primary source of heat flux observations is the New Global Heat Flow (NGHF) compilation [32], which is augmented in the US by the SMU Node of the National Geothermal Data System [2].

NGHF is the most recent compilation of global heat flux measurements since Pollack, Hurter, and Johnson [35]. It contains about 40,000 continental measurements globally. Most heat flux observations in NGHF are from borehole measurements of heat conductivity and temperatures at multiple depths from the surface to a few hundred meters (**eq.** (3)). It is conventional to define geothermal heat flux, q, as the conductive flux in the upward direction near the Earth surface:

$$q \equiv k \left. \frac{\partial T}{\partial z} \right|_{z=0}, \tag{3}$$

where k denotes heat conductivity, and T temperature, both varying with depth z in general.

For the contiguous US (**Fig. 2**a–c), the SMU data augments the NGHF in the Central and Eastern US, especially with bottom hole temperature measurements across parts of the Great Plains and the Midwestern US. The bottom hole temperature measurements can have both good and poor qualities; on the one hand, the measurements can extend to much greater depths ($>$ 1500 m) than typical geothermal holes (a few hundred meters); on the other hand, conductivity is seldom measured directly, and is often prescribed based on geological information of specific areas [36]. However, the data sources provide little information about data quality. These measurements are spatially dense enough to compare neighboring locations to one another, which turn out to vary spatially less than traditional geothermal measurements (**Fig. 2**b).

2.1.2 Quality control

Due to the absence of information about the quality of heat flux observations, we perform our own quality control which involves data rejection, imputation, and spatial smoothing.

The observed heat flux q^{obs} based on **eq.** (3) is the sum of the true heat flux q_0 and measurement errors ϵ, and can be written as $q^{\text{obs}} = q_0 + \epsilon$. Moreover, q_0 can be approximated as the result of regional background heat flux, q_R (with a spatial scale R) perturbed by small-scale variations δq, such that $q_0 = q_R + \delta q$. Perturbations δq may come from paleoclimate, sedimentation and erosion, seismicity, and ground water circulation [37]. Since our interest

is q_R, the unwanted part is $\Delta q \equiv \delta q + \epsilon$. Therefore,

$$q^{\text{obs}} = q_R + \Delta q. \tag{4}$$

The resolution of seismic tomography limits $R \sim 100$ km, which requires removing small-scale variations in heat flux before investigating the relationship between seismic structure and heat flux. Unfortunately, most values do not have associated quantitative uncertainties ϵ, nor are they corrected for near-surface effects that control δq. Thus, we apply the following criteria to down-weigh measurements that we believe to have large δq or ϵ.

First, we eliminate observations outside the range from $10\,\text{mW/m}^2$ to $150\,\text{mW/m}^2$. This is because the lower limit of mantle heat flux is typically larger than $10\,\text{mW/m}^2$ [38], while values higher than $150\,\text{mW/m}^2$ are commonly associated with geothermal reservoirs [39]. Second, we remove observations made at depths < 100 m, because shallower depths are affected by climate oscillations with periods shorter than century scales (assuming thermal diffusivity $\kappa \approx 1\ \text{mm}^2/\text{s}^2$). Third, we compute standard deviations, s, for a set of observations within a 10 km radius, and reject all of the observations within this set if $s > 20\,\text{mW/m}^2$. This is because large variations with spatial scales shorter than 10 km are unlikely to be explained by seismic structure with resolution ∼100 km. The threshold value of s is significantly larger than typical ϵ. Specifically, among the 1549 continental measurements with ϵ provided by NGHF, the median of ϵ is $5\,\text{mW/m}^2$ and its MAD is $6\,\text{mW/m}^2$.

To remove small-scale variations and to alleviate the spatially uneven sampling of raw observations, we smooth observations twice. First, we average point observations within a 10 km distance on a 10-km grid. Then the median (**Fig. 2**ad) and MAD (**Fig. 2**be) are computed for these local means across a 100 km radius, producing a heat flux map on a 100-km grid.

In the US, heat flux observations from the Snake River Plain [**Brott˙etal˙1981**] and South Dakota [40] are known to be dominated by hydrothermal circulations. Therefore, we replace heat flux observations with $90\,\text{mW/m}^2$ for the Snake River Plain [**Brott˙etal˙1981**],

and 60 mW/m^2 for South Dakota [40], which are more representative of regional heat flux values.

To assign a quality estimate, which we refer to as a weight w, to each point of the heat flux map, we do the following. The median heat flux values are weighed by both the associated MAD, w_{MAD}, and the misfit from a smooth model prediction, w_{misfit}, such that the total weight is the product of these two weights,

$$w = w_{\text{MAD}} \cdot w_{\text{misfit}}. \tag{5}$$

Both w_{MAD} and w_{misfit} for the i-th heat flux median value are defined as

$$w_i = \min\left(1, \left(n\frac{\text{MAD}(x)}{x_i}\right)^2\right), \tag{6}$$

where we choose $n = 2$. If the data are normally distributed, then this choice of n will down-weight the outer 5% of data. For w_{MAD}, the variable x denotes the MAD of heat flux within a 100 km radius, $x_i = \text{MAD}(\{q_j^{\text{obs}} : |r_j - r_i| < 100 \text{ km}\})$. For w_{misfit}, the variable x denotes the absolute difference between heat flux observations and (smooth) predictions, $x_i = |\hat{q}_i - q_i^{\text{obs}}|$. The smooth model prediction is from a Decision Tree with a level of 3 (**section 3.1.2**). The final weights are presented in **Fig. 2**cf. The median heat flux values and their associated weights are the input data to models, corresponding to q^{obs}, w in **eq.** (1), respectively. These weights are used to define the misfit between model predictions and heat flux observations (**section 4**).

2.1.3 Spatial patterns of heat flux

The US heat flux shows a west-east dichotomy, which reflects fundamentally distinct tectonic regimes of the western and eastern US. This dichotomy is basic for any model to reproduce heat flux from seismic structure. Specifically, the western US hs higher values and the eastern US has lower values, with intermediate values in the Great Plains (**Fig. 2**a).

Regionally, high anomalies are observed in the Basin and Range, and the Rio Grande rift; while low anomalies are shown in the Cascadia subduction zone, the Colorado Plateau, and much of the eastern US except near the Appalachian Mountains. These regional-scale variations are the central goal of our model to reproduce.

We compute MAD values of heat flux observations within a 100 km radius. Large MAD values of heat flux mostly correspond to high values in the western US (**Fig. 2**b). Given this radius of 100 km is much larger than the natural variability of heat flux, MAD values measure not only observation uncertainty, but also spatial variability. In particular, large MAD values can be caused by averaging across values of contrast such as along the Cascade Range, while small MAD values across the central US may suggest either the high quality of the bottom hole temperature measurements there or the uniformity in prescribed heat conductivity.

European heat flux observations in NGHF are mostly based on a compilation by Cermak and Rybach [41]. Heat flux in Europe shows a northwest-southeast dichotomy, divided by the Trans-European Suture Zone (**Fig. 2**d). High heat flux values are observed in the Massif Central and the Upper Rhine Plain, east of the Dinarides and Hellenides, and in Anatolia, while low values are measured in the Baltic Shield, the Russian Platform, the Apennines, and the Dinarides and Hellenides. The North Germain Plain has intermediate heat flux.

The MAD values of heat flux are generally larger in Europe than the US, although the US data have more exceptionally large values (**Fig. 2**e). This means that the European heat flux observations have larger spatial variability than the US data on a 100 km scale. Large MAD values of European heat flux also correlate with high heat flux values, especially along the Alps.

2.2 Seismic structure

We focus on seismic structure as a proxy for heat flux for the following reasons. First, seismic structure is sensitive to temperature and composition as functions of depth which

fundamentally determine heat flux [42]. Second, a significant correlation has been observed between seismic structure and heat flux [24, 35, 43]. Third, seismic observations provide one of the highest-resolution images of the solid Earth structure.

2.2.1 Sources of information

The US seismic structural information is from Shen and Ritzwoller [33] (**Fig. 5**a–c), which represents the state of the art in continental seismic tomography. This information uses the seismic data from the EarthScope USArray, including Rayleigh wave dispersion and amplitudes (ellipticity), and body wave converted phases (receiver functions). In particular, Rayleigh waves are measured from both earthquakes and ambient noise, which complements earthquakes at higher frequencies to constrain crustal structure. At each target location, a seismic shear wavespeed profile V_S is parameterized with three "layers" from the surface to 150 km depth: a sediment layer in which V_s increases linearly with depth, a crustal layer where V_S varies smoothly with depth, and a mantle layer where V_S also changes smoothly with depth. Discontinuities can exist between the layers. Posterior distributions of profile parameters are presented, which are determined via a Bayesian approach with Markov Chain Monte Carlo sampling. The inferred seismic shear wavespeed is actually V_{SV}, but we refer to it as V_S here.

The European seismic tomography result is from Lu, Stehly, and Paul [34, **Fig. 5**d–f], which is based on data mainly from the AlpArray. They adopt a similar methodology as Shen and Ritzwoller [33] so we only discuss the main differences. First, they use Rayleigh waves only from ambient noise and only measure group speed. Second, their model is parameterized with four constant layers from the surface to 80 km depth: a sedimentary layer, an upper crust, a lower crust, and an uppermost mantle. Third, they construct a posterior distribution at each location with a Bayesian approach, but their final model is a linear inversion of the posterior mean. These differences in data types, parameterization, and inversion strategies can manifest as inconsistencies between the seismic structural variables, which we discuss in

sections 2.2.2 and **2.2.3**.

2.2.2 Selection of seismic structural variables

While the seismic structure is a continuous function of depth at each location, we deliberately choose a few seismic variables to characterize a seismic profile for two reasons. First, seismic structural information can differ systematically from diverse methods by various groups, so they might not be directly comparable. Second, seismic inversions suffer from trade-offs between the parameters, so we seek a set of seismic structural variables that correlate the least with each other.

To identify a few variables that are representative of the whole structure, we perform a hierarchical clustering with Ward variance minimization (**Fig. 4**). For both the US and Europe seismic structural variables, we identify three clusters that correspond to the crust, the crust-mantle transition zone, and the uppermost mantle. Thus, we use the shear wavespeed at 15 km depth to represent the crust, shear wavespeed at 65 km depth for the uppermost mantle, and the Moho depth for the crust-mantle boundary (**Fig. 5**). The visual similarity between seismic structure and heat flux is striking for V_S at 65 km depth (**Fig. 5**be). These three variables essentially characterize a seismic structural profile with two constant layers. This small number of variables leads to a simple model, which is more likely to be interpretable and transportable than a model involving a large number of variables.

2.2.3 Standardization of seismic structural variables

The statistical distributions of these three seismic structural variables are significantly different between the US and Europe (**Fig. 5**g–i). Thus, we standardize a seismic structural variable by subtracting its spatial mean across each continent and then dividing it by its spatial standard deviation. The mean and standard deviation account for the systematic differences (e.g. due to parameterization) and relative variations (e.g. due to varied resolution) of the seismic structural variables, respectively. These standardized variables are part of the

input to the models, corresponding to v_i in **eq.** (1).

2.3 Summary of input data to Machine Learning models

The description of data in this section specifies the input variables to Machine Learning models in **eq.** (1). The q^{obs} and w refer to the heat flux and associated weights on a 100 km grid respectively (**section 2.1**), while $v(r, z)$ denotes the three seismic structural variables after standardization: the V_S at 15 km depth, V_S at 65 km depth, and the Moho depth (**section 2.2**). We discuss the models themselves next (**section 3.1**).

3 Methods

In this section, we first describe the three Machine Learning models considered in this study (**section 3.1**), which characterize the relationship between seismic structure and surface heat flux. These models are the Linear Regression model (**section 3.1.1**), the Decision Tree model (**section 3.1.2**), and the Random Forest model (**section 3.1.3**).

We then present the variation of model accuracy with complexity (**section 3.2**). This illustrates the fundamental trade-off between model bias (under-fitting of data) and variance (over-fitting of data) for a Machine Learning model. We discuss this bias-variance trade-off based on validation (**section 3.2.1**) and cross-validation (**section 3.2.2**), which we use to evaluate the accuracy and transportability of these models, respectively.

3.1 Machine Learning models across a hierarchy of complexity

We choose these three models because they model heat flux across a hierarchy of spatial scales, from continental scale (Linear Regression), to regional scale (Decision Tree), and local scale (Random Forest). In this context, the complexity of the models, is essentially equivalent to their spatial resolution, and number of model parameters (which may be different in other contexts).

Each Machine Learning model is specified by model parameters θ and hyper-parameters $\tilde{\theta}$, which together constitute all the parameters of a model, $\Theta = \{\theta, \tilde{\theta}\}$ (**eq.** (1)). Model parameters are derived via fitting model predictions to data, while model hyper-parameters are defined by the user and cannot be inferred from data fitting. We will specify the parameters and hyper-parameters of each of the three models, i.e., the Linear Regression model (**section 3.1.1**), the Decision Tree model (**section 3.1.2**), and the Random Forest model (**section 3.1.3**).

We use the weighted root mean squared error (RMSE) to quantify data misfit for all models,

$$\mathrm{RMSE}(\hat{q}) \equiv \left(\sum_{i=1}^{N_{\mathrm{obs}}} w_i' (\hat{q}_i - q_i^{\mathrm{obs}})^2 \right)^{\frac{1}{2}}, \tag{7}$$

where $\hat{q}_i \equiv \hat{q}(r_i)$, w_i' denotes the normalized weight, $w_i' = w_i / \sum_{k=1}^{N_{\mathrm{obs}}} w_k$, w_i is defined in **section 2.1.2**, r_i denotes spatial locations, and N_{obs} denotes the number of heat flux observations defined on a 100 km grid.

3.1.1 Linear Regression

As a baseline reference, we consider the Linear Regression model,

$$\hat{q}_i = c_0 + \sum_{j=1}^{N_v} c_j v_{i,j}, \tag{8}$$

where $\hat{q}_i \equiv \hat{q}(r_i)$, r_i denotes spatial locations, $v_{i,j}$ denotes the j-th seismic variable of $v(r_i)$ (the V_S at 15 km depth, V_S at 65 km depth, and the Moho depth), $N_v = 3$ denotes the number of seismic structural variables, and c_j are the coefficients that define a line ($j = 0, 1, 2, 3$). For the Linear Regression model, the model parameters θ are c_j, and there are no model hyper-parameters $\tilde{\theta}$.

The Linear Regression model can be straight-forwardly interpreted based on its coefficients, c_j. However, the coefficients are fit to the whole area, i.e., they are the same for a continent. Thus, the Linear Regression model cannot distinguish the *regional* differences

in the relationship (e.g. tectonically active versus stable). One could address this issue by fitting a Linear Regression model to each region, but this regionalization information needs to be provided *a priori*, and cannot be derived from the model itself. We discuss how the Decision Tree and Random forest models can overcome this issue by obtaining regionalization *a posteriori*.

We implement the Linear Regression model with the `LinearRegression` module of `scikit-learn` [44].

3.1.2 Decision Tree

3.1.2.1 Motivation and heuristics

A priori, we would expect a tectonically active region to have high temperature and low seismic wavespeed, and thus high heat flux. Conversely, we may relate high heat flux with such variables. This regionalization information has to be provided to a Linear Regression model *a priori*, which motivates us to develop the Decision Tree model to obtain regionalization *a posteriori*.

The Decision Tree model [e.g. 45] yields a set of *decision rules*, each of which links a specific type of seismic structure with a constant heat flux. Specifically, without knowledge of any seismic structural variable $v^{(i)}$, it is sensible to make a trivial prediction, $\hat{q}^{(0)}$, as the weighted average of all observed heat flux values, $\bar{q}^{\text{obs}}$,

$$\hat{q}^{(0)} = \bar{q}^{\text{obs}} = \sum_{i=1}^{N_{\text{obs}}} w_i' q_i^{\text{obs}}. \tag{9}$$

This builds a Decision Tree with a level L of 0: $L \equiv 0$, and corresponds to the root node upon which any further level of the Decision Tree builds.

As a concrete example, consider building a Decision Tree for the US data. The root node corresponds to the first row of the tree in **Fig. 10**, which makes the trivial prediction of a constant heat flux with the continental average of $\hat{q}^{(0)} = 57\,\text{mW/m}^2$ (**eq.** (9)).

Given a seismic structural variable, $v^{(1)}$, the data can be split into two disjoint subsets by a threshold value of this variable, $v_*^{(1)}$. Then two constant predictions can be made by taking the average heat flux observations of the two subsets. These are the two decision rules generated by this Decision Tree of level $L = 1$. An optimal variable is the one whose predictions have the least RMSE (**eq.** (7)).

For example, consider again the Decision Tree built from the US data but with the first two rows. This corresponds to a level of 1: $L = 1$. The second row in **Fig. 10** denotes splitting the data with the V_S at 65 km depth: $v^{(1)} = \text{Vs\_065}$. The splitting threshold is 4.36 km/s: $v_*^{(1)} = 4.36$ km/s. The standardized threshold value is -0.46. The two decision rules are: (1) if the location has uppermost mantle wavespeed slower than this threshold, $v^{(1)} \leq v_*^{(1)}$, then assign a higher heat flux of $\hat{q} = 70\,\text{mW/m}^2$; (2) otherwise, if the location has uppermost mantle wavespeed faster than this threshold, $v^{(1)} > v_*^{(1)}$, then assign a lower heat flux of $\hat{q} = 51\,\text{mW/m}^2$.

Intriguingly, the first and second rules correspond to the Western and Eastern US, respectively (**Fig. 12**a). This revelation of the east-west tectonic dichotomy of the US suggests that the first-order variation in heat flux is predicted by the uppermost mantle V_S (rather than the crustal structure or crustal thickness). The uppermost mantle V_S is likely affected by temperature more than other factors such as composition and partial melt [e.g. 43], which further indicates a control by uppermost mantle temperature and thermal lithosphere thickness.

This simple example illustrates the main advantage of the Decision Tree model—its splitting of data tends to coincide with geological provinces (despite no geographical locations being given), which can reveal *regional* variations in the relationship between seismic structure and heat flux. It thus shows promise to illuminate heat flux variations at smaller spatial scales by adding further splits thereby growing the tree. We present Decision Trees with levels up to $L = 3$ in **section 4.1**.

3.1.2.2 Precise definition

In the previous section, we describe a Decision Tree with a level $L = 1$ and only a single splitting. Each of the two parts from this split can be further partitioned by a second split, via a seismic structural variable that may or may not be the same as $v^{(1)}$ or each other. This generates a Decision Tree with a level of $L = 2$ and a total of 4 decision rules. In general, a Decision Tree with a level L can have at most a total of 2^L decision rules.

To be more precise, a prediction $\hat{q}$ is sequentially refined based on one seismic structural variable at a time,

$$\hat{q} = \hat{q}^{(0)} + \delta\hat{q}^{(1)}\left(\mathrm{sgn}(v^{(1)} - v_*^{(1)})\right) + \delta\hat{q}^{(2)}\left(\mathrm{sgn}(v^{(2)} - v_*^{(2)})\right) + \cdots \tag{10}$$

where $v^{(L)}, L = 1, 2, \ldots$ denote the seismic structural variable in the L-th level, sgn denotes a sign function, and $\delta\hat{q}^{(L)}, L = 1, 2, \ldots$ are binary functions with two possible outputs. The absolute values or amplitudes of $\delta\hat{q}^{(i)}$ are generally (but not necessarily) smaller than $\hat{q}^{(0)}$ and decrease with level L. Thus, one could roughly think of the splitting process as adding "higher-order corrections".

In other words, consider the 3-D space, β, spanned by the three ($N_v = 3$) seismic structural variables v_k. The decision rules partition this space β into a total of N_β disjoint blocks β^α: $\beta = \cup_{\alpha=1}^{N_\beta}\beta^\alpha$, where $\beta^\alpha \cap \beta^\gamma = \emptyset$ if $\alpha \neq \gamma$. Let $\lfloor v_k^\alpha \rfloor$ and $\lceil v_k^\alpha \rceil$ denote the lower and upper limits of the k-th ($k = 1, 2, \cdots, N_v$ and $N_v = 3$ here) seismic variable v_k associated with the α-th block ($\alpha = 1, 2, \cdots, N_\beta$), respectively. Each block β^α is specified as where the seismic variables are within these limits: $\beta^\alpha = \{v | \lfloor v_k^\alpha \rfloor \leq v_k \leq \lceil v_k^\alpha \rceil, k = 1, 2, \cdots, N_v\}$. Therefore, the seismic structural variables at a spatial location, v_i, are uniquely identified within a block

β^α, which is assigned with a constant heat flux value $\bar{q}^\alpha$:

$$\begin{aligned} \hat{q}_i &= \sum_{\alpha=1}^{N_\beta} \bar{q}^\alpha \mathbf{1}_{\beta^\alpha}(v_i), \\ \bar{q}^\alpha &= \sum_{k=1}^{N_{\text{obs}}} w_k^\alpha q_k^{\text{obs}} \mathbf{1}_{\beta^\alpha}(v_k), \end{aligned} \tag{11}$$

where $w_k^\alpha = w_k / \sum_{j=1}^{N_{\text{obs}}} w_j \mathbf{1}_{\beta^\alpha}(v_j)$ denotes weights (**eq.** (5)), $\hat{q}_i \equiv \hat{q}(r_i), v_i \equiv v(r_i), q_k^{\text{obs}} \equiv q^{\text{obs}}(r_k)$, $\mathbf{1}$ is an indicator function,

$$\mathbf{1}_{\beta^\alpha}(v) = \begin{cases} 1, & \text{if } v \in \beta^\alpha, \\ 0, & \text{if } v \notin \beta^\alpha. \end{cases} \tag{12}$$

For the Decision Tree model, the model parameters θ are splitting variables and associated thresholds, $v_*^{(i)}$ (**eq.** (10)), while we choose the model hyper-parameter $\tilde{\theta}$ as the maximum level of the tree, L.

We implement the Decision Tree model with the `DecisionTreeRegressor` module of `scikit-learn` [44].

3.1.3 Random Forest

A Random Forest is an ensemble of Decision Trees and is designed to avoid over-fitting [46]. This is achieved by using a random subset of both heat flux observations and seismic structural variables to train each tree, and then combining all the trees for prediction.

For the Random Forest model, the model parameters are the splitting variables and associated thresholds for each tree, while the model hyper-parameter is chosen by us to be the total number of trees.

Since a Random Forest typically consists of more than tens of trees, it operates somewhat like a black box where the explicit linkage from seismic structure to heat flux is highly complicated. It is, therefore, not effective at illuminating how a specific heat flux prediction

is made from seismic structural variables.

We implement the Random Forest model with the `RandomForestRegressor` module of `scikit-learn` [44].

3.2 Evaluation of model accuracy and transportability

3.2.1 Validation for model accuracy

To optimize model hyper-parameters and validate prediction uncertainties, we should train the model on one set of data (the training set) and then validate on a separate set of data (the validation set).

Here, we partition the heat flux observations into an 80% training set and a 20% complementary validation set. We then train a model on the training data, and compare its predictions to the validation data. This process is repeated using a total of 20 different random partitions of the data.

3.2.1.1 Fit to validation data

To determine the accuracy or predictive power of the models, we evaluate the goodness of fit to the heat flux data using the coefficient of determination, r^2, which measures the proportion of observed heat flux variations predicted by each model:

$$r^2(\hat{q}) \equiv 1 - \frac{\sum_{i=1}^{N_{\text{obs}}} w_i'(q_i^{\text{obs}} - \hat{q}_i)^2}{\sum_{i=1}^{N_{\text{obs}}} w_i'(q_i^{\text{obs}} - \bar{q}^{\text{obs}})^2} = 1 - \left(\frac{\text{RMSE}}{\sigma^{\text{obs}}}\right)^2, \tag{13}$$

where $\bar{q}^{\text{obs}}$ denotes the average value across the heat flux map (**eq.** (9)), w_i' denotes the normalized weight (**section 2.1.2**), σ^{obs} denotes the spatial standard deviation of q^{obs}, RMSE is defined in **eq.** (7), and $r^2 \in (-\infty, 1]$. In particular, if $\hat{q}_i = \bar{q}^{\text{obs}}$, then $r^2 = 0$; if $\hat{q}_i = q_i^{\text{obs}}$, then $r^2 = 1$. It is instructive to put in some realistic numbers. Assume $\sigma^{\text{obs}} = 15\,\text{mW/m}^2$, which is close to both the US and European data (**Fig. 3**). Thus, $r^2 = 0, 0.5, 0.75$ for

RMSE $= 15, 11, 7.5\,\mathrm{mW/m^2}$ respectively. Since r^2 is a linear function of the mean squared error (RMSE^2), their relative variations with model hyper-parameters are the same. Therefore, using either r^2 or least squares will yield the same choices of optimal model hyper-parameters.

The r^2 on validation data provides an estimate of model accuracy. For example, each error bar in **Fig. 6** denotes the mean and standard deviation of r^2 from validating the Decision Tree model with a specific max level L. The relative r^2 for different hyper-parameters (e.g. max level L for a Decision Tree) serves as a basis for choosing the optimal hyper-parameter, which we elaborate below.

3.2.1.2 Hyper-parameter choices

We illustrate how hyper-parameters are chosen with the Decision Tree models (**Fig. 6**). The structure of a Decision Tree is controlled by its maximum level L. The training performance of a Decision Tree increases monotonically with L, which is simply caused by a better fit to the data by adding model parameters. In contrast, the validation score of a tree first increases with L until $L = 5$ but then plateaus/decreases, as a result of transitioning from under-fitting to over-fitting. Moreover, the validation scores are more variable than training scores, probably because a larger fraction of data are repeated in training. Thus, we choose $L = 3$ as a compromise between fitting the data while keeping the model interpretable. In particular, increasing the level from 3 to 4 will approximately double the number of decision rules from $\sim$8 to $\sim$16.

We choose the number of tress to be 10 for the Random Forest model (**Fig. S2**).

3.2.2 Cross-validation for model transportability

To evaluate the transportability of a model, we apply each of the US-trained models to the European data, and vice versa. The results from this cross-validation are discussed in **section 4.2**.

We introduce another metric besides r^2 to measure the *geographical coherence* between

heat flux predictions and observations. This is because r^2 measures the overall misfit (**eq.** (13)), and thus includes the amplitudes of the observations as well as the geographical pattern. We introduce the Pearson's correlation coefficient ρ, which is less sensitive to the absolute amplitudes. Specifically, ρ measures the linear (in)dependence between predictions $\hat{q}$ and observations q^{obs},

$$\rho(\hat{q}) \equiv \frac{\text{Cov}(\hat{q}, q^{\text{obs}})}{\hat{\sigma}\sigma^{\text{obs}}}, \tag{14}$$

where Cov denotes the covariance, $\hat{\sigma}$ and σ^{obs} denote the spatial standard deviation of predicted and observed heat flux, respectively, and $\rho \in [-1, 1]$. In particular, if the predictions are linearly related to the observations, $\hat{q}_i = kq_i^{\text{obs}} + b$ where k, b are constants and $k > 0$, then $\rho = 1$, while r^2 can be low if $k \neq 1$ or $b \neq 0$. If $\hat{q}_i$ is a constant, then $\rho = 0$, while $r^2 = 0$ only if $\hat{q}_i = \bar{q}^{\text{obs}}$ (**eq.** (9)), and $r^2 < 0$ otherwise.

4 Results

In this section, we first address the characterization problem using data from the same continent (**section 4.1**), which includes evaluation of model accuracy from validation (**section 4.1.1**) and the resulting improvement in understanding of the relationship between seismic structure and heat flux (**section 4.1.2**). Then we tackle the transportability problem by applying the US-trained model to the European data, and vice versa (**section 4.2**). This includes evaluation of model transportability by model cross-validation (**section 4.2.1**) and the resulting insight gained about challenges in transporting models between continents (**section 4.2.2**).

4.1 Characterization within the same continent

We first develop our method in the best-case scenario, where both heat flux and seismic structural data are from the same continent. This is because we expect greater consistency between the training and validation data in the US than between the US and European data. More consistent data will produce more accurate models.

4.1.1 Comparison of model accuracy

We compare the three models in terms of accuracy and spatial variability both qualitatively by visually comparing maps (**Figs** 8 and 9) and quantitatively through statistical measures (**Fig.** 7) and maps (**Figs** 8 and 9). The statistical analyses provide a summary of the details on the maps.

The model statistics are summarized in **Fig.** 7a for the US data alone. The Random Forest model has the best scores, but its validation performance ($r^2 = 0.66 \pm 0.03$) is much worse than its training performance ($r^2 = 0.95 \pm 0.00$), which indicates over-fitting (**Fig.** 8e). The validation performance of the Decision Tree model is comparable ($r^2 = 0.63 \pm 0.02$) to that of the Random Forest, but its training score ($r^2 = 0.68 \pm 0.01$) is much closer to its own validation score, which suggest that it is less prone to over-fitting than the Random Forest model. The Linear Regression model performs slightly worse ($r^2 = 0.52 \pm 0.03$) than the Decision Tree and Random Forest models.

The relative performance of the models is similar using the European data alone (**Fig.** 7b). However, the r^2 values are generally lower, which suggests that heat flux can be better explained by seismic structure in the US than in Europe.

We also preasent model accuracy and spatial variability in map form (**Fig.** 8). For each of the three models, our 20%/80% (validation/training) splitting of training and validation data with 20 folds (**section** 3.2.1) means that every location on average is predicted four times as validation data. We randomly choose a unique prediction for each location (**Fig.** 8a–c), and compare them with observations (**Fig.** 8d). The Linear Regression predictions are the most smooth (**Fig.** 8a), because the coefficients are fit to the whole area and thus are not sensitive to subsetting the data (**Fig.** S3). In contrast, the Decision Tree predictions are more accurate but also are more spatially variable (**Fig.** 8b), which is caused by its hard splits at threshold values of seismic structural variables, and its weak sensitivity subsetting the data. The Random Forest predictions are the most spatially variable (**Fig.** 8c), because of its strong sensitivity to data subsetting as it attempts to fit all local data variations.

These models exhibit similar spatial variability for the European data alone (**Fig. 9**). However, the European predictions generally have larger differences with observations. Thus, the European predictions are less accurate, consistent with their lower statistics (**Fig. 7**).

In summery, the Decision Tree model fits the validation data equally well as the Random Forest model and slightly better than the Linear Regression model. Moreover, the Decision Tree model illuminates the regional variations of the relationship between heat flux and seismic structure, while the other two models cannot. Therefore, we focus the following insights on the region-specific relationship from the Decision Tree model (**section 4.1.2**).

4.1.2 Insights from the Decision Tree model

We clarify here the region-specific relationship between seismic structure and heat flux by visualizing the Decision Tree structure (**Figs 10** and **13**), the associated decision rules (**Figs 11** and **14**), the map view of ruled regions (**Figs 12** and **15**), and the relative importance of seismic structural variables (**Fig. 16**).

We use three levels in the Decision Tree ($L = 3$), and retrain a Decision Tree model using all data from the US alone to discover the most general relationship between heat flux and seismic structure in the US (**Figs 10** to **12**). To avoid over-fitting, we require that each of the two parts from a splitting has at least 5% of the total data. We also repeat the process to build a Decision Tree using all the European data (**Figs 13** to **15**).

In the US, a single splitting of a Decision Tree reveals the west-east dichotomy of heat flux (**Fig. 12**a), which manifests as a bimodal distribution of V_S at 65 km depth (**Fig. 11** bottom row). As we further grow the tree by increasing its level L, we start to see regional variations finer than the west-east dichotomy (**Fig. 12**bc). Specifically, across the Western US, the highest heat flux values are correlated with very slow uppermost mantle wavespeeds in the Basin and Range, and the Rio Grande Rift (**Fig. 11**ab). High heat flux values surrounding the Colorado Plateau are characterized by a slow crustal wavespeed (**Fig. 11**c), while relatively low heat flux values within the Colorado Plateau correlate with fast/intermediate

crustal wavespeed (**Fig. 11**d). In the Eastern US, heat flux values are generally lower than those in the West and are associated with fast uppermost mantle wavespeed (**Fig. 11**e–g). Relatively high heat flux values are associated with either a thick crust in the Great Plains and Appalachian Mountains (**Fig. 11**f), or slow crustal wavespeed in the Mississippi Embayment (**Fig. 11**c). The lowest heat flux values in the Eastern US correlate with regions having thin crust and fast crustal wavespeed (**Fig. 11**g).

Most large misfits are correlated with large spatial variability of heat flux observations even before these regions are down-weighted (**Fig. 2**b). These include undershooting (predictions smaller than observations) at the Basin and Range, the Rio Grande Rift, and South Dakota; and the overshooting at Yellowstone. These regions also host hydrothermal systems [39, 40]. We do not understand large MAD values and residuals at the Southern Appalachians. Prediction overshoots at the Cascade Range, which is undergoing active subduction and is therefore tectonically distinct from elsewhere in the US.

In Europe, we find that the northeast-southwest dichotomy of heat flux is anti-correlated with uppermost mantle V_S, roughly separated by the Trans-European Suture Zone between the Precambrian East European Craton and the Phanerozoic Southwest European orogens (**Fig. 15**). Moreover, the highest heat flux is correlated with a very slow uppermost mantle (e.g. Massif Central, east of Dinarides and Hellenides) or a thin crust (e.g. Upper Rhine Plain; **Fig. 14**a). The lowest heat flux values are characterized by a fast uppermost mantle, and a thick crust (the Baltic Shield, Russian Platform, Apennines, and Dinarides and Hellenides; **Fig. 14**gh). Intermediate heat flux at the North German Plain is mostly anti-correlated with crustal thickness (**Fig. 14**de).

Similar to the US data, large misfits often correlate with large MAD values of heat flux observations (**Fig. 2**d). These include the undershooting at France and Anatolia; and the overshooting at the Apennines.

To quantify the relative importance of seismic structural variables, we compute the variance reduction from each seismic structural variable, normalizing the total reduction as unity

(Gini importance). For the US data, this shows that the uppermost mantle contributes about 80% of the variance reduction, while the crust V_S and Moho depth each accounts for around 10% (**Fig. 16**).

For the European data, uppermost mantle V_S still dominates while crustal V_S is secondary. However, the Moho depth is more important than in the US. A comparison of the decision rules suggest that the Moho depth is positively related with heat flux in the US (**Fig. 11**fg), but negatively in Europe (**Fig. 11**f–h). This is consistent with the Linear Regression model, where the coefficients for the Moho depth have opposite signs and different relative magnitudes (**Fig. S3**).

These tree structures, rules, and maps from growing the number of levels of the Decision Tree illustrate the unique advantage of the Decision Tree model. It tends to split the whole area into regions corresponding with geological provinces, despite no such geographical information being given. Moreover, it can yield a specific relationship between heat flux and seismic structure for each region. These region-specific relationships constitute our answer to most of the characterization problem, which we summarize below (**section 4.1.3**).

4.1.3 Summary for the characterization problem

We find that seismic structure can explain more than half of the observed heat flux variations in both the US and Europe (**Figs 7** to **9**). We discuss potential reasons for the unexplained heat flux variations ($> 30\%$) in **section 5.1.1**. Uppermost mantle wavespeed is the primary predictor of heat flux, while crustal wavespeed and Moho depth are secondary (**Fig. 16**). The region-specific relationship between seismic structure and heat flux is explicitly characterized by several decision rules (**Figs 10** to **15**). The Random Forest and Decision Tree models are more accurate than the Linear Regression model.

We note two differences using the US and European data. First, the US heat flux observations are better explained by seismic structure than the European observations. Second, the Moho depth plays a more important role for the European data than the US data. We

discuss potential causes for these two differences in **section 5.1.3** and **section 5.1.2**, respectively. These differences will affect transporting the models from one continent to the other, which we discuss next (**section 4.2**).

4.2 Transporting models from one continent to the other

In continents where heat flux observations are rare or absent (such as Antarctica), the model cannot be trained with local heat flux observations. Therefore, the scenario in **section 4.1** is inapplicable, and the model has to be trained on other continents where heat flux observations exist. To evaluate how our models will perform in this more challenging case, we apply the US-trained models to the European data, and vice versa.

4.2.1 Comparison of model transportability

We compare the transportability of the three models using both statistics (**Fig. 17**) and in map form (**Figs 18** and **19**).

We apply each of the three models trained in the US to the European data and summarize their metrics in **Fig. 17**a. The Linear Regression and Decision Tree models have the best overall misfit ($r^2 \approx 0.2$), while the Random Forest model is significantly worse ($r^2 = -0.05$). As discussed above (**section 4.1.1**), the Random Forest model is prone to over-fitting, as suggested by small scale variations in its heat flux predictions (**Fig. 18**c).

The relative performance of the models in geographical coherence (ρ) is similar to performance in overall misfit (r^2). However, the absolute values of ρ are about 0.3 larger than r^2 for all three models ($\rho \approx 0.5$ for the Decision Tree and Linear Regression models, and $\rho \approx 0.3$ for the Random Forest model). This means the prediction of the geographical patterns of heat flux is better than the overall fit to the data, which is degraded by the models' limitations in fitting amplitudes.

These model comparisons are consistent with applying the Europe-trained models to the US data (**Fig. 17**b). However, the values of both metrics are higher for transporting from

Europe to the US than from US to Europe (r^2 increases about 0 to 0.2, ρ increases about 0.2 to 0.3). This is consistent with better model accuracy using the US data alone than the European data alone (**section 4.1.1**).

For both the US and European data, the misfit values are significant worse than using data from the same continent (**Fig. 7**) for all three models (r^2 reduces about $0.2, 0.4$, and 0.6 for the Linear Regression, Decision Tree, and Random Forest models, respectively). This suggests that model transportability deteriorates with increasing spatial resolution.

We also present model transportability in map form (**Fig. 18**), where we compare predictions (**Fig. 18**a–c) with observations (**Fig. 18**d). The Linear Regression and Decision Tree model predictions have similar spatial variability as observations, while the Random Forest model predictions show noisy local variations. Compared to predictions using the European data alone (**Fig. 9**), the geographical patterns are similar, but the absolute amplitudes tend to be under-predicted from all three models.

These models exhibit similar spatial variability when the Europe-trained models are applied to the US data (**Fig. 19**). However, the absolute amplitudes tend to be over-predicted, compared to the US-trained models (**Fig. 8**).

These metrics and maps suggest that the geographical patterns of heat flux observations can be reasonably predicted by the Decision Tree and Linear Regression models (and to a lesser extent by the Random Forest model), but the absolute amplitudes cannot by any of the three models. Because the Decision Tree model can uniquely identify region-specific relationships between seismic structure and heat flux, we use the Decision Tree model to discuss the differences in transporting the relationship from one continent to the other in the next section (**section 4.2.2**).

4.2.2 Insights from the Decision Tree models

We compare the US-trained Decision Tree model (**Figs 10** to **12**) with the Europe-trained Decision Tree model (**Figs 13** to **15**), and discuss how differences between predictions and

observations emerge when applying the US-trained models to the European data (**Fig. 20**), and vice versa (**Fig. 21**).

The Decision Tree model trained with the US data alone is able to delineate the northeast-southwest European tectonic dichotomy based on uppermost mantle wavespeed, where high heat flux is related to a slow uppermost mantle in the Massif Central, east of the Dinarides and Hellenides, and Anatolia (**Fig. 20**a). Relative high heat flux is associated with slow crustal wavespeed for the rest of southwest Europe (**Fig. 20**b).

The US-trained model, however, mistakenly assigns higher heat flux at the eastern Baltic Shield and the Russian Platform than the western Baltic Shield (**Fig. 20**c). This is because the eastern Baltic Shield has a thick crust and similar seismic structure to the Central US (higher heat flux), while the western Baltic Shield has a thinner crust and similar seismic structure to the eastern US (lower heat flux). Moreover, both models trained in the US (**Fig. 20**) and Europe (**Fig. 15**) cannot fit the exceptionally high heat flux in France. While Cenozoic volcanism can explain high values at the Massif Central, relatively high values in the Paris Basin are not well understood [41].

The Decision Tree model trained with the European data alone can identify the west-east US tectonic dichotomy based on uppermost mantle wavespeed. In this dichotomy, high heat flux is related to a slow uppermost mantle in the western US, while low heat flux is related to a fast uppermost mantle in the eastern US (**Fig. 21**a). Relative high heat flux is associated with a relatively thin crust in the Mississippi Embayment, while relative low heat flux is associated with a relatively thick crust in the eastern US (**Fig. 21**b).

The Europe-trained model, however, wrongly assigns higher heat flux at Florida than the Central US (**Fig. 21**c). This is because Florida has a relatively thin crust and seismic structure similar to the North Germany Basin (higher heat flux), while the Central US has a thick crust and similar seismic structure to the Baltic Shield (lower heat flux). Furthermore, models trained either in the US (**Fig. 20**) or Europe (**Fig. 15**) cannot fit the exceptionally low heat flux in the Cascade Range region, which is undergoing active subduction.

These comparisons provide key insights for the transportability problem, which we summarize below (**section 4.2.3**).

4.2.3 Summary for the transportability problem

We find that the geographical coherence of heat flux can be reasonably reproduced from one continent to the other (**Fig. 17**). In particular, the Europe-trained models can better predict the US data, than vice versa. Exceptions are mostly for relatively low heat flux values, which we discuss in **section 5.1.5**. The Linear Regression and Decision Tree models are more transportable than the Random Forest model.

The absolute amplitudes of variations, however, are under-predicted in Europe when using the US models (**Fig. 20**), and over-predicted in the US when using the European models (**Fig. 21**). We discuss this in **section 5.1.6**.

In addition to potential reasons for these differences, we also discuss the implications for heat flux inferences across Antarctica in **section 5.1**.

5 Discussion

Given the emergence of new information about the seismic structure of the crust and uppermost mantle beneath Antarctica [47, 48], the methods we present hold promise to improve the reliability and resolution of the inferences of heat flux across Antarctica. The validation and cross-validation of our method against existing heat flux observations in the US and Europe (**section 4**) provide insights for transporting heat flux to Antarctica. We now summarize these insights and discuss their implications for predicting heat flux across Antarctica (**section 5.1**). We also illustrate applications of our methodology to validate heat flux proxies other than seismic structure (**section 5.2**).

5.1 Implications for heat flux inference across Antarctica

5.1.1 Unexplained heat flux variations within a continent

Even using data from the same continent, a significant fraction of heat flux variations are not explained by seismic structure in either the US ($r^2 < 0.7$) or Europe ($r^2 < 0.6$; **Fig. 7**). This means that dissimilar seismic structure can be linked to similar heat flux values and vice versa. We attribute the unexplained 30% to 40% variations mainly to crustal radiogenic heat production. This is because heat production can dominate heat flux, but its relationship with seismic structure is weak [38]. For example, an empirical relationship is proposed by Pollack and Chapman [49] which attributes ∼40% of observed heat flux to upper crustal radiogenic sources and the remaining ∼60% to any deeper source (radiogenic sources in the lower crust, heat flux from the mantle, etc.). This empirical 40%/60% partition is established from several provinces including the Basin and Range, the Eastern US, and the Baltic Shield [49].

Current knowledge of crustal radiogenic heat production in Antarctica is highly localized, most of which is near the periphery of Antarctica where outcrops occur [**Sanchez˙etal˙2021a**]. Heat production is likely to continue to be a fundamental factor that limits the accuracy of heat flux inference across Antarctica from both seismic structure and other proxies for years to come.

5.1.2 Relative importance of seismic structural variables

We find that the uppermost mantle V_S is the primary predictor of heat flux, while the crustal V_S and Moho depth are secondary (**Fig. 16**). Specifically, both the west-east dichotomy in the US and the northeast-southwest dichotomy in Europe are illuminated by the uppermost mantle V_S. This provides quantitative evidence for the correlation between uppermost mantle V_S and heat flux proposed by earlier studies [9, 24, 35, 43]. However, the Moho depth is relatively more important in Europe, especially for lower heat flux values.

We note that the uppermost mantle V_S and the Moho depth are positively correlated in the Apennines, the Dinarides, and the Baltic Shield (**Fig. 5**ef), at length scales which we believe are below the resolution of the seismic data. This suggests that these structures are not independently estimated in the European seismic structural information from Lu, Stehly, and Paul [34].

To determine heat flux values on a continental scale representative for West versus East Antarctica, the uppermost mantle mantle V_S in Antarctica could be used as the main predictor. This west-east dichotomy (higher heat flux in West Antarctica and lower heat flux in East Antarctica) has been identified by many previous studies, but the amplitude of the dichotomy remains uncertain [31].

5.1.3 Better prediction of the US data than the European data

For predictions within each continent (**Fig. 7**) or between the two continents (**Fig. 17**), the US heat flux is better predicted than the European heat flux. This suggests that either heat flux is more directly related with seismic structure in the US than Europe, the quality of information about heat flux and/or seismic structure is better in the US than those in Europe, or crustal radiogenic heat production is stronger in Europe than in the US.

In any case, the more accurate relationship between heat flux and seismic structure suggests giving more weight to the US data (heat flux, seismic structure) than the European data when transporting heat flux to Antarctica.

5.1.4 Trade-off between model complexity and transportability

We find that the Decision Tree and Random Forest models are the most accurate based on validation within each continent (**Fig. 7**), while the Decision Tree and Linear Regression models are the most transportable from cross-validation between the two continents (**Fig. 17**). This is because the Linear Regression and Decision Tree models fit heat flux variations on continental and regional scales, while the Random Forest model tends to over-fit

variations by extending them to a local scale. Compared to the Linear Regression model, the Decision Tree model additionally provides insight about the regionalization of heat flux observations on the scale of geological provinces.

Therefore, the Decision Tree model is recommended over the Linear Regression model for transporting heat flux to Antarctica, and the Random Forest model should be avoided.

5.1.5 Difficulty in predicting the geographical patterns between continents

When transporting models between the US and Europe, the geographical coherence of heat flux is overall well reproduced, but with exceptions in a few locations (**section 4.2.2**). This means that similar seismic structure can be linked with different heat flux values, which violates the operational assumption that underlies the use of seismic structure as a heat flux proxy: that similar seismic structural information should be related with similar heat flux values. A notable example lies in Northeast Europe, and its counterpart in the Central and Eastern US, where the Moho depth is negatively and positively related with heat flux, respectively.

Assuming heat flux observations are reliable, this may be caused by differences in the US and Europe resulting from (1) the seismic structural imaging methods or (2) crustal radiogenic heat production.

(1) As we point out in **section 5.1.2**, significant trade-offs between the Moho depth and uppermost mantle V_S may exist in the European seismic structural information [34]. Transportability would improve if seismic structure is estimated similarly for both continents, for example by using the same types of data and parameterization.

(2) As discussed in **section 5.1.1**, the relationship between crustal radiogenic heat production and seismic structure is probably weak [38]. A log-linear relationship between heat production and V_P has been discovered, but the relationship varies between different rock types, geologic ages, and geological provinces [**RybachBuntebarth˙1984**, **HasterokWebb˙2017**]. Therefore, different heat production in the US and Europe can link similar seismic structure

with dissimilar heat flux, which is caused by differences in rock types, geologic ages, and geological provinces. This results in errors in the prediction of the geographic pattern of heat flux between the two continents. In the future, geological information (rock type, age, and province) can complement seismic structural information to better constrain heat production and thus heat flux predictions between continents.

We note that the seismic data and parameterization of Shen et al. [47] in Antarctica is the same as those used by Shen and Ritzwoller [33] in the US. In contrast, the European seismic structure imaged by Lu, Stehly, and Paul [34] is based on a different approach. Therefore, the seismic structural information from the US may be more appropriate for inferring heat flux in Antarctica than that from Europe, if the seismic structure of Shen et al. [47] is to be used in Antarctica. Moreover, geological information can complement seismic structural information for future prediction of heat flux across Antarctica.

5.1.6 Difficulty in predicting the absolute amplitudes between continents

When transporting models between the US and Europe, we find that the absolute amplitudes are over-predicted in the US (**Fig. 19**) and under-predicted in Europe (**Fig. 18**).

The statistical distributions of heat flux are different in the US and Europe, where the European data show more variability (higher highs, lower lows) despite Europe's smaller area (**Fig. 3**). We asses whether absolute amplitudes can be better predicted by standardizing the heat flux distributions on each continent separately. Specifically, for heat flux data on each continent, we remove the mean and divide by the standard deviation. The standard deviaton of heat flux across Europe is about 30% larger than across the US. We find that this standardization does not change the geographical coherence (ρ), but improves the prediction of absolute amplitudes and reduces the overall misfit (r^2 increase about 0.1 to 0.2; **Fig. S6**).

The larger variability of heat flux data in Europe is caused by the US data being more peaked at intermediate values and the European data being more heavy-tailed, particularly at the high heat flux end of the distribution (**Fig. 2**). We are not certain whether this is caused

by intrinsic differences in heat flux between the continents, or by errors in the measurements of heat flux.

The statistical distribution of heat flux across Antarctica is not currently known. The difference of about 30% in the variability of heat flux between Europe and the US is a valuable guide to the expected differences in the absolute amplitudes of heat flux predictions for Antarctica.

5.1.7 Summary for transporting heat flux from the US and Europe to Antarctica

For inferring heat flux across Antarctica, we suggest that the US data (heat flux, seismic structural information) should be given more weight than the European data because heat flux data can be predicted from seismic structure more accurately in the US than in Europe (**section 5.1.3**). In addition, the US seismic structural information is parameterized more similarly to that in Antarctica (**section 5.1.5**). However, the European data could be incorporated to improve predictions of the absolute amplitudes of heat flux (**section 5.1.6**). We recommend using the uppermost mantle V_S as the primary predictor (**section 5.1.2**). We also recommend the Decision Tree model for its transportability and geologically relevant regionalization (**section 5.1.4**). We suggest that crustal radiogenic heat production is a prominent systematic uncertainty, which can cause at least 30% of heat flux variations which are not predictable by seismic structure (**sections 5.1.1** and **5.1.5**). In the future, geological information can complement seismic structural information to better constrain heat production and thus heat flux across Antarctica. This inference of heat flux across Antarctica is pursued in our ongoing work [**ZhangRitzwoller˙2023**].

5.2 Validation of proxies other than seismic structure

Our validation and cross-validation methodology can also be applied to validate proxies other than seismic structure. For example, we use the magnetic Curie depth below [18, 21], but this procedure is also applicable to other heat flux proxies such as surface topography

[29].

Heat flux inferences based on magnetic anomalies within a region begin by estimating the Curie depth Z_b. Then they typically assume an exponential decay of heat production with depth z: $H(z) = H_0 \exp(-z/h_r)$, where H_0 is the surface heat production, and h_r is the characteristic depth of heat production. We note that whether $H(z)$ follows an exponential function is generally uncertain [38, 39]. Assuming 1-D steady state, the following relationship has been obtained between the Curie depth Z_b, Curie temperature T_c, and surface heat flux $\hat{q}$ [e.g. 21]:

$$\hat{q} = -k\frac{T_c}{Z_b} - H_0 h_r \left[1 - \frac{h_r}{Z_b}\left(1 - \exp\left(-\frac{Z_b}{h_r}\right)\right)\right], \tag{15}$$

where k denotes heat conductivity.

For most places in the world and especially Greenland and Antarctica [**Sanchez˙etal˙2021a**], heat production $H(z)$ is poorly known [38], and perhaps to a lesser extent so are k, T_c. However, because magnetic anomaly data are also available in the US and Europe [**Maus˙etal˙2009**], heat flux observations from these two continents can be used to validate this relationship. In particular, the characterization on the same continent can determine the predictive power of this relationship and calibrate the model parameters such as k, H_0, h_r (**section 4.1**). Moreover, the transportability of this relationship can be measured by cross-validation between the US and Europe (**section 4.2**).

6 Conclusion

The characterization and transportability problems defined and addressed in this study are motivated by the importance of estimating heat flux beneath polar ice sheets, and the inconsistency that exists between previous heat flux estimates based on proxy data in these regions (**section 1.1**).

To investigate the characterization and transportability problems, we directly compare predictions and observations of surface heat flux using data from the US and Europe. We

apply quality control on heat flux heat flux observations by data rejection, imputation and smoothing (**section 2.1**). Moreover, we identify three principal seismic structural variables (uppermost mantle V_S, crustal V_S, and Moho depth) to represent seismic structure in both the US and Europe, using a clustering analysis (**section 2.2**). We find that further complications in the seismic structure do not improve the ability to predict heat flux appreciably. Our analysis focuses on using three Machine Learning models across a hierarchy of complexity to determine the relationship between these three structural variables and surface heat flux (**section 3**).

To address the characterization problem, we train the Machine Learning models with the training data and then validate the models with the validation data within the same continent. We find that uppermost mantle V_S is the strongest predictor of heat flux and is considerably more important than crustal V_S and Moho depth (**section 4.1**). However, crustal V_S and Moho depth are relatively more important in tectonically stable regions (i.e., eastern US and northern Europe). Together, these three variables explain more than half of heat flux observations (r^2 about 50% to 60% in Europe and the US, respectively). We attribute the unexplained heat flux variations ($> 30\%$) mainly to crustal radiogenic heat production. This is because heat production can greatly affect heat flux but may not be strongly sensitive to seismic structure [38].

To tackle the transportability problem, we apply the models trained on the US data to predict heat flux across Europe, and vice versa (**section 4.2**). While performing this cross-validation between the two continents, we find that the Decision Tree and Linear Regression models are more transportable than the Random Forest model. The Decision Tree and Linear Regression models can reasonably reproduce the geographic distribution of heat flux, but to a lesser extent reproduce the absolute amplitudes of heat flux variations. The US heat flux is better predicted from the Europe-trained models, than vice versa.

Given the recent emergence of high-resolution seismic structural information for Antarctica [47, 48], the methodology presented in this paper promises to improve the reliability and

resolution of inferences of heat flux across Antarctica. We suggest that the US data should be given more weight than the European data in transporting models of the relationship between seismic structure and heat flux, because this relationship is more accurate in the US (**section 5.1.3**). Moreover, the parameterization of seismic structure in the US is more similar to that in Antarctica (**section 5.1.5**). However, the European data can be incorporated to improve predictions of the absolute amplitudes of heat flux variations (**section 5.1.6**). We recommend the use of the Decision Tree model for its transportability and correlation with geological provinces (**section 5.1.4**). Uppermost mantle V_S emerges from the Decision Tree model as the primary predictor of heat flux (**section 5.1.2**). We suggest that crustal radiogenic heat production is a prominent systematic uncertainty, which can cause at least 30% of heat flux variations (**sections 5.1.1** and **5.1.5**).

Our method can also be applied to validate distinct models of the relationship between heat flux and proxies other than seismic structure [e.g. 18, 19, 29]. This validation is crucial to help resolve existing inconsistencies between heat flux inferences for Antarctica based on different proxies (**section 5.2**). This improvement of the inference of heat flux beneath Antarctica, and the potential resolution of existing inconsistencies, would improve constraints on the subglacial thermal boundary conditions, and thereby lead to more accurate predictions of the future evolution of ice sheets and their contributions to future sea level change.

Data Availability

Geothermal heat flux observations are based on NGHF [32], and the SMU Node of the National Geothermal Data System [http://geothermal.smu.edu/gtda; 2]. The US seismic structural information is from Shen and Ritzwoller [33], and the European structure is from Lu, Stehly, and Paul [34]. Codes to reproduce this study will be made available on `GitHub` upon acceptance of the manuscript.

Funding

This research is supported by a CIRES Graduate Student Research Award (SZ) and NSF grant EAR-1943112 (MHR, SZ) at the University of Colorado Boulder.

Acknowledgements

We acknowledge helpful discussions with Billy Shinevar, Kyle Goodrick, and Derek Mease. We thank Francis Lucazeau for providing the NGHF data, SMU Geothermal Lab for maintaining the SMU Node of the National Geothermal Data System, Weisen Shen for the US seismic structure, and Yang Lu for the European seismic structure.

References

[1]C. Jaupart and J. .-. Mareschal, "6.05 - Heat Flow and Thermal Structure of the Lithosphere", *Treatise on Geophysics (Second Edition)*, edited by G. Schubert (Elsevier, Oxford, 2015), pp. 217–253.

[2]D. Blackwell, M. Richards, Z. Frone, J. Batir, A. Ruzo, R. Dingwall, and M. Williams, "Temperature-At-Depth Maps for the Conterminous U. S. and Geothermal Resource Estimates", GRC Transactions, 7 (2013).

[3]A. H. Lachenbruch and B. V. Marshall, "Changing Climate: Geothermal Evidence from Permafrost in the Alaskan Arctic", Science **234**, 689–696 (1986).

[4]D. Pollard, R. M. DeConto, and A. A. Nyblade, "Sensitivity of Cenozoic Antarctic Ice Sheet Variations to Geothermal Heat Flux", Global and Planetary Change **49**, 63–74 (2005).

[5]M. Llubes, C. Lanseau, and F. Rémy, "Relations between Basal Condition, Subglacial Hydrological Networks and Geothermal Flux in Antarctica", Earth and Planetary Science Letters **241**, 655–662 (2006).

[6]F. Pattyn, "Antarctic Subglacial Conditions Inferred from a Hybrid Ice Sheet/Ice Stream Model", Earth and Planetary Science Letters **295**, 451–461 (2010).

[7]I. Rogozhina, J. M. Hagedoorn, Z. Martinec, K. Fleming, O. Soucek, R. Greve, and M. Thomas, "Effects of uncertainties in the geothermal heat flux distribution on the Greenland Ice Sheet: An assessment of existing heat flow models", Journal of Geophysical Research: Earth Surface **117** (2012).

[8]T. L. Noble, E. J. Rohling, A. R. A. Aitken, H. C. Bostock, Z. Chase, N. Gomez, L. M. Jong, M. A. King, A. N. Mackintosh, F. S. McCormack, R. M. McKay, L. Menviel, S. J. Phipps, M. E. Weber, C. J. Fogwill, B. Gayen, N. R. Golledge, D. E. Gwyther, A. M. C. Hogg, Y. M. Martos, B. Pena-Molino, J. Roberts, T. van de Flierdt, and T. Williams, "The

Sensitivity of the Antarctic Ice Sheet to a Changing Climate: Past, Present and Future", Reviews of Geophysics **n/a**, e2019RG000663 (2020).

[9]N. M. Shapiro and M. H. Ritzwoller, "Inferring Surface Heat Flux Distributions Guided by a Global Seismic Model: Particular Application to Antarctica", Earth and Planetary Science Letters **223**, 213–224 (2004).

[10]R. Greve, "Relation of Measured Basal Temperatures and the Spatial Distribution of the Geothermal Heat Flux for the Greenland Ice Sheet", Annals of Glaciology **42**, 424–432 (2005/ed).

[11]C. Fox Maule, M. E. Purucker, and N. Olsen, "Inferring Magnetic Crustal Thickness and Geothermal Heat Flux from Crustal Magnetic Field Models", Danish Climate Center Report (2009).

[12]A. G. Petrunin, I. Rogozhina, A. P. M. Vaughan, I. T. Kukkonen, M. K. Kaban, I. Koulakov, and M. Thomas, "Heat Flux Variations beneath Central Greenland's Ice Due to Anomalously Thin Lithosphere", Nature Geoscience **6**, 746–750 (2013).

[13]S. Rezvanbehbahani, L. A. Stearns, A. Kadivar, J. D. Walker, and C. J. van der Veen, "Predicting the Geothermal Heat Flux in Greenland: A Machine Learning Approach", Geophysical Research Letters **44**, 12, 271–12, 279 (2017).

[14]Y. M. Martos, T. A. Jordan, M. Catalán, T. M. Jordan, J. L. Bamber, and D. G. Vaughan, "Geothermal Heat Flux Reveals the Iceland Hotspot Track Underneath Greenland", Geophysical Research Letters **45**, 8214–8222 (2018).

[15]I. M. Artemieva, "Lithosphere Thermal Thickness and Geothermal Heat Flux in Greenland from a New Thermal Isostasy Method", Earth-Science Reviews **188**, 469–481 (2019).

[16]S. Rezvanbehbahani, L. A. Stearns, C. J. van der Veen, G. K. A. Oswald, and R. Greve, "Constraining the Geothermal Heat Flux in Greenland at Regions of Radar-Detected Basal Water", Journal of Glaciology, 1–12 (2019).

[17]W. Colgan, A. Wansing, K. Mankoff, M. Lösing, J. Hopper, K. Louden, J. Ebbing, F. G. Christiansen, T. Ingeman-Nielsen, L. C. Liljedahl, J. A. MacGregor, Á. Hjartarson, S. Bernstein, N. B. Karlsson, S. Fuchs, J. Hartikainen, J. Liakka, R. S. Fausto, D. Dahl-Jensen, A. Bjørk, J.-O. Naslund, F. Mørk, Y. Martos, N. Balling, T. Funck, K. K. Kjeldsen, D. Petersen, U. Gregersen, G. Dam, T. Nielsen, S. A. Khan, and A. Løkkegaard, "Greenland Geothermal Heat Flow Database and Map (Version 1)", Earth System Science Data **14**, 2209–2238 (2022).

[18]C. Fox Maule, M. E. Purucker, N. Olsen, and K. Mosegaard, "Heat Flux Anomalies in Antarctica Revealed by Satellite Magnetic Data", Science **309**, 464–467 (2005).

[19]B. Goutorbe, J. Poort, F. Lucazeau, and S. Raillard, "Global Heat Flow Trends Resolved from Multiple Geological and Geophysical Proxies", Geophysical Journal International **187**, 1405–1419 (2011).

[20]M. An, D. A. Wiens, Y. Zhao, M. Feng, A. Nyblade, M. Kanao, Y. Li, A. Maggi, and J.-J. Lévêque, "Temperature, Lithosphere-Asthenosphere Boundary, and Heat Flux beneath the Antarctic Plate Inferred from Seismic Velocities", Journal of Geophysical Research: Solid Earth **120**, 8720–8742 (2015).

[21]Y. M. Martos, M. Catalán, T. A. Jordan, A. Golynsky, D. Golynsky, G. Eagles, and D. G. Vaughan, "Heat Flux Distribution of Antarctica Unveiled", Geophysical Research Letters **44**, 11, 417–11, 426 (2017).

[22]A. Burton-Johnson, J. A. Halpin, J. M. Whittaker, F. S. Graham, and S. J. Watson, "A New Heat Flux Model for the Antarctic Peninsula Incorporating Spatially Variable Upper Crustal Radiogenic Heat Production", Geophysical Research Letters **44**, 5436–5446 (2017).

[23]A. Pollett, D. Hasterok, T. Raimondo, J. A. Halpin, M. Hand, B. Bendall, and S. McLaren, "Heat Flow in Southern Australia and Connections With East Antarctica", Geochemistry, Geophysics, Geosystems **20**, 5352–5370 (2019).

[24]W. Shen, D. Wiens, A. Lloyd, and A. Nyblade, "A Geothermal Heat Flux Map of Antarctica Empirically Constrained by Seismic Structure", Geophysical Research Letters **n/a**, e2020GL086955 (2020).

[25]S. N. P. Guimarães, F. P. Vieira, and V. M. Hamza, "Heat Flow Variations in the Antarctic Continent", International Journal of Terrestrial Heat Flow and Applied Geothermics **3**, 1–10 (2020).

[26]R. Dziadek, F. Ferraccioli, and K. Gohl, "High Geothermal Heat Flow beneath Thwaites Glacier in West Antarctica Inferred from Aeromagnetic Data", Communications Earth & Environment **2**, 1–6 (2021).

[27]M. Lösing and J. Ebbing, "Predicting Geothermal Heat Flow in Antarctica With a Machine Learning Approach", Journal of Geophysical Research: Solid Earth **126**, e2020JB021499 (2021).

[28]T. Stål, A. M. Reading, J. A. Halpin, and J. M. Whittaker, "Antarctic Geothermal Heat Flow Model: Aq1", Geochemistry, Geophysics, Geosystems **22**, e2020GC009428 (2021).

[29]I. M. Artemieva, "Antarctica Ice Sheet Basal Melting Enhanced by High Mantle Heat", Earth-Science Reviews **226**, 103954 (2022).

[30]C. Haeger, A. G. Petrunin, and M. K. Kaban, "Geothermal Heat Flow and Thermal Structure of the Antarctic Lithosphere", Geochemistry, Geophysics, Geosystems **23**, e2022GC010501 (2022).

[31]A. Burton-Johnson, R. Dziadek, and C. Martin, "Geothermal Heat Flow in Antarctica: Current and Future Directions", The Cryosphere **14**, 3843–3873 (2020).

[32]F. Lucazeau, "Analysis and Mapping of an Updated Terrestrial Heat Flow Data Set", Geochemistry, Geophysics, Geosystems **20**, 4001–4024 (2019).

[33]W. Shen and M. H. Ritzwoller, "Crustal and Uppermost Mantle Structure beneath the United States", Journal of Geophysical Research: Solid Earth **121**, 4306–4342 (2016).

[34]Y. Lu, L. Stehly, and A. Paul, "High-Resolution Surface Wave Tomography of the European Crust and Uppermost Mantle from Ambient Seismic Noise", Geophysical Journal International **214**, 1136–1150 (2018).

[35]H. N. Pollack, S. J. Hurter, and J. R. Johnson, "Heat Flow from the Earth's Interior: Analysis of the Global Data Set", Reviews of Geophysics **31**, 267 (1993).

[36]D. D. Blackwell and M. C. Richards, "The 2004 Geothermal Map of NOrth America", Geothermal Resources Council Transactions **28** (2004).

[37]W. G. Powell, D. S. Chapman, N. Balling, and A. E. Beck, "Continental Heat-Flow Density", Handbook of Terrestrial Heat-Flow Density Determination: with Guidelines and Recommendations of the International Heat-Flow Commission, 167–222 (1988).

[38]C. Jaupart, J.-C. Mareschal, and L. Iarotsky, "Radiogenic Heat Production in the Continental Crust", Lithos **262**, 398–427 (2016).

[39]A. H. Lachenbruch and J. H. Sass, "Heat Flow in the United States and the Thermal Regime of the Crust", *The Earth's Crust* (American Geophysical Union (AGU), 1977), pp. 626–675.

[40]W. D. Gosnold, "Heat Flow in the Great Plains of the United States", Journal of Geophysical Research: Solid Earth **95**, 353–374 (1990).

[41]V. Cermak and L. Rybach, *Terrestrial Heat Flow in Europe*, Vol. 58 (Springer Science & Business Media, 1979).

[42]N. M. Shapiro and M. H. Ritzwoller, "Thermodynamic Constraints on Seismic Inversions", Geophysical Journal International **157**, 1175–1188 (2004).

[43]A. H. E. Röhm, R. Snieder, S. Goes, and J. Trampert, "Thermal Structure of Continental Upper Mantle Inferred from S-wave Velocity and Surface Heat Flow", Earth and Planetary Science Letters **181**, 395–407 (2000).

[44]F. Pedregosa, G. Varoquaux, A. Gramfort, V. Michel, B. Thirion, O. Grisel, M. Blondel, P. Prettenhofer, R. Weiss, V. Dubourg, J. Vanderplas, A. Passos, D. Cournapeau, M. Brucher, M. Perrot, and É. Duchesnay, "Scikit-Learn: Machine Learning in Python", Journal of Machine Learning Research **12**, 2825–2830 (2011).

[45]L. Breiman, J. H. Friedman, R. A. Olshen, and C. J. Stone, *Classification and Regression Trees* (Routledge, 2017).

[46]L. Breiman, "Random Forests", Machine Learning **45**, 5–32 (2001).

[47]W. Shen, D. A. Wiens, S. Anandakrishnan, R. C. Aster, P. Gerstoft, P. D. Bromirski, S. E. Hansen, I. W. D. Dalziel, D. S. Heeszel, A. D. Huerta, A. A. Nyblade, R. Stephen, T. J. Wilson, and J. P. Winberry, "The Crust and Upper Mantle Structure of Central and West Antarctica From Bayesian Inversion of Rayleigh Wave and Receiver Functions", Journal of Geophysical Research: Solid Earth **123**, 7824–7849 (2018).

[48]A. J. Lloyd, D. A. Wiens, H. Zhu, J. Tromp, A. A. Nyblade, R. C. Aster, S. E. Hansen, I. W. D. Dalziel, T. Wilson, E. R. Ivins, and J. P. O'Donnell, "Seismic Structure of the Antarctic Upper Mantle Imaged with Adjoint Tomography", Journal of Geophysical Research: Solid Earth **125**, 10.1029/2019JB017823 (2020).

[49]H. N. Pollack and D. S. Chapman, "On the Regional Variation of Heat Flow, Geotherms, and Lithospheric Thickness", Tectonophysics **38**, 279–296 (1977).

Figures

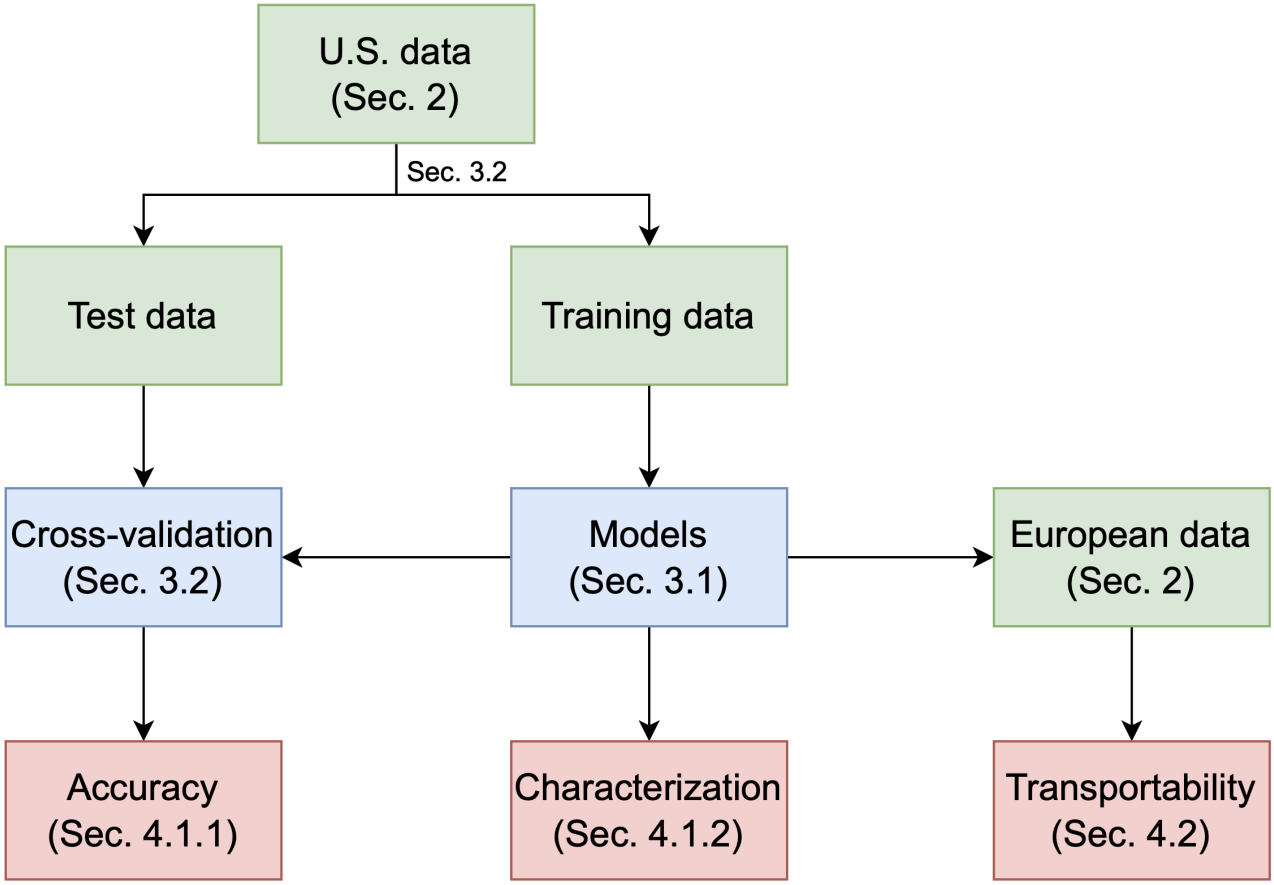

Figure 1: **An overview of the logical flow of this paper.** Data, methods, and results are color-coded in green, blue, and red, respectively. The US data (heat flux, seismic structure) are split into training and validation data. The Machine Learning models are trained with the training data and then validated with the validation data for accuracy. The models specify the relationship between heat flux and seismic structure which addresses the characterization problem. The US-trained models are then cross-validated against the European (EU) data to tackle the transportability problem. The Europe-trained models are also transported to the US data by switching the role of the US and European data.

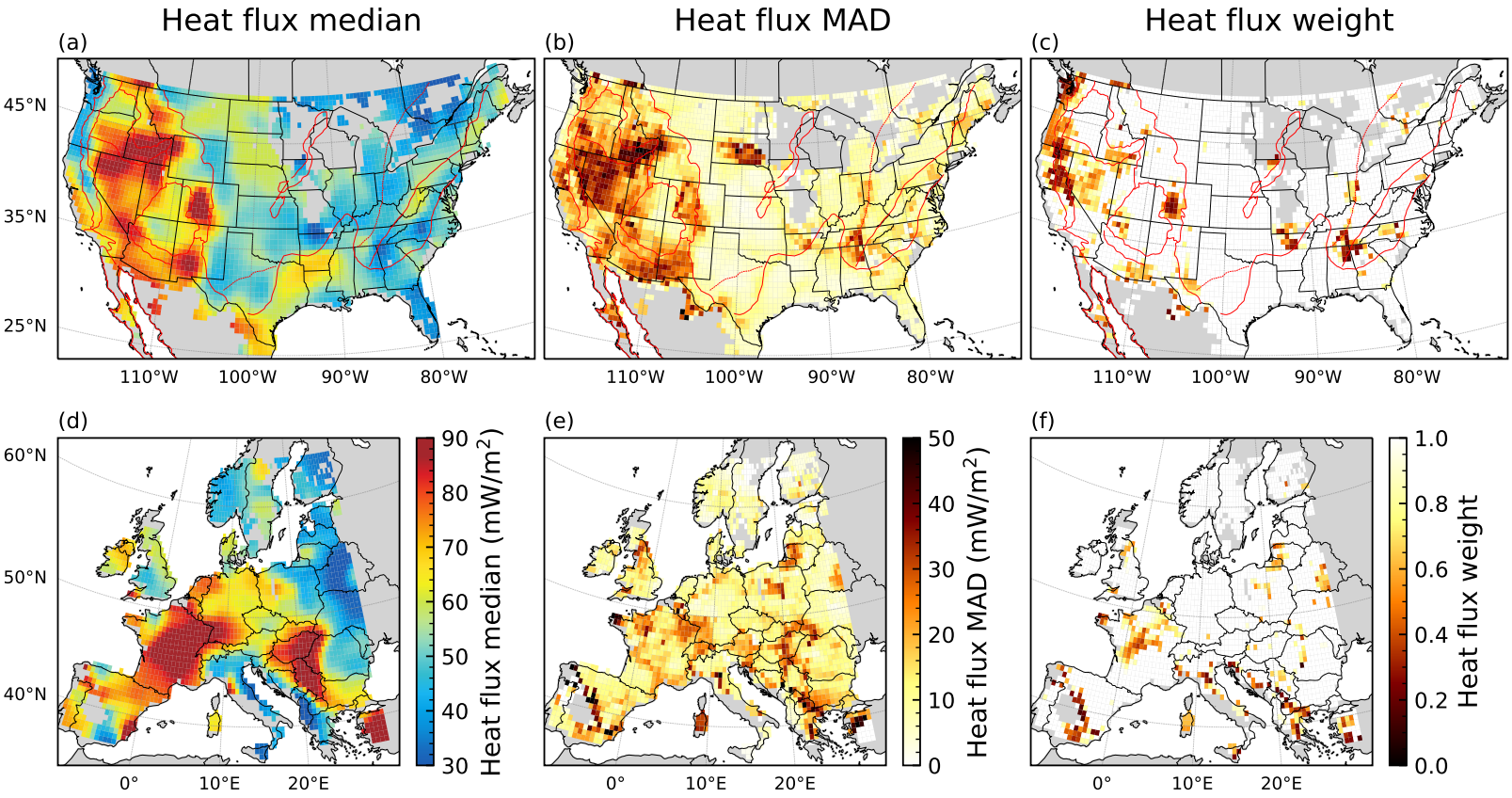

Figure 2: **Heat flux observations.** (a)–(c) Heat flux observations are smoothed onto a 100 km grid to match seismic structural resolution across the contiguous US. (a) The median values of heat flux within a 100 km radius, q^{obs}, are shown. (b) The MAD (Median Absolute Deviation) values of heat flux within a 100 km radius are shown, which is a robust measure of spatial variability (**eq.** (2)). (c) The weights, w, of median values are shown, such that regions with large MAD or misfit to a smooth model are down-weighted (**eq.** (5)). The median values, q^{obs}, and weights, w, are part of the input data to the Machine Learning models (**eq.** (1)). (d)–(f) Similar to (a)–(c) but for European heat flux.

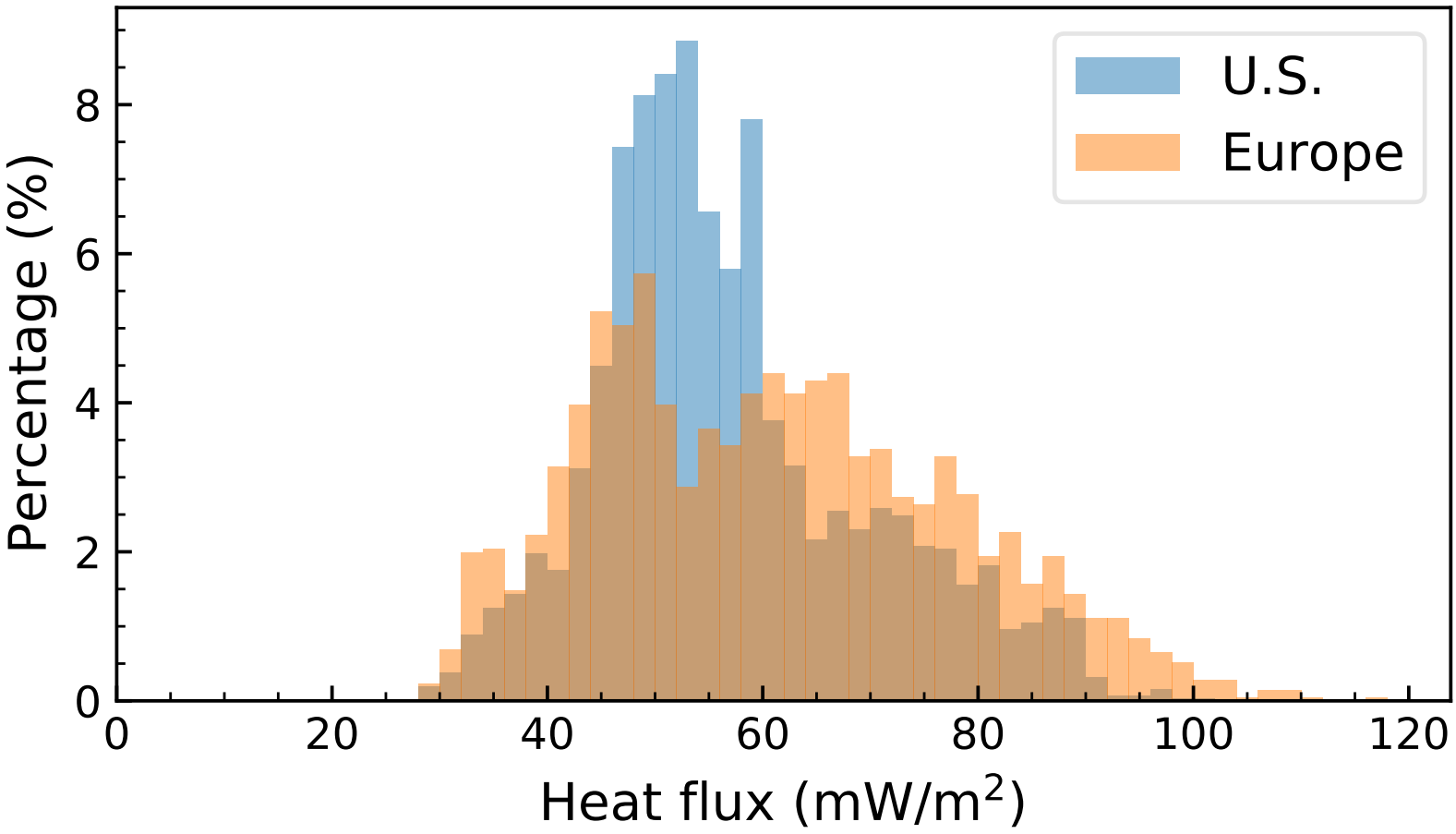

Figure 3: **Distributions of heat flux observations.** Histograms of heat flux values for the US data (blue) and European data (orange) from the smoothed maps (**Fig. 2**a & d). The European data are distributed more broadly (higher highs, lower lows), which affects the prediction of the absolute amplitudes of heat flux when transporting between the two continents.

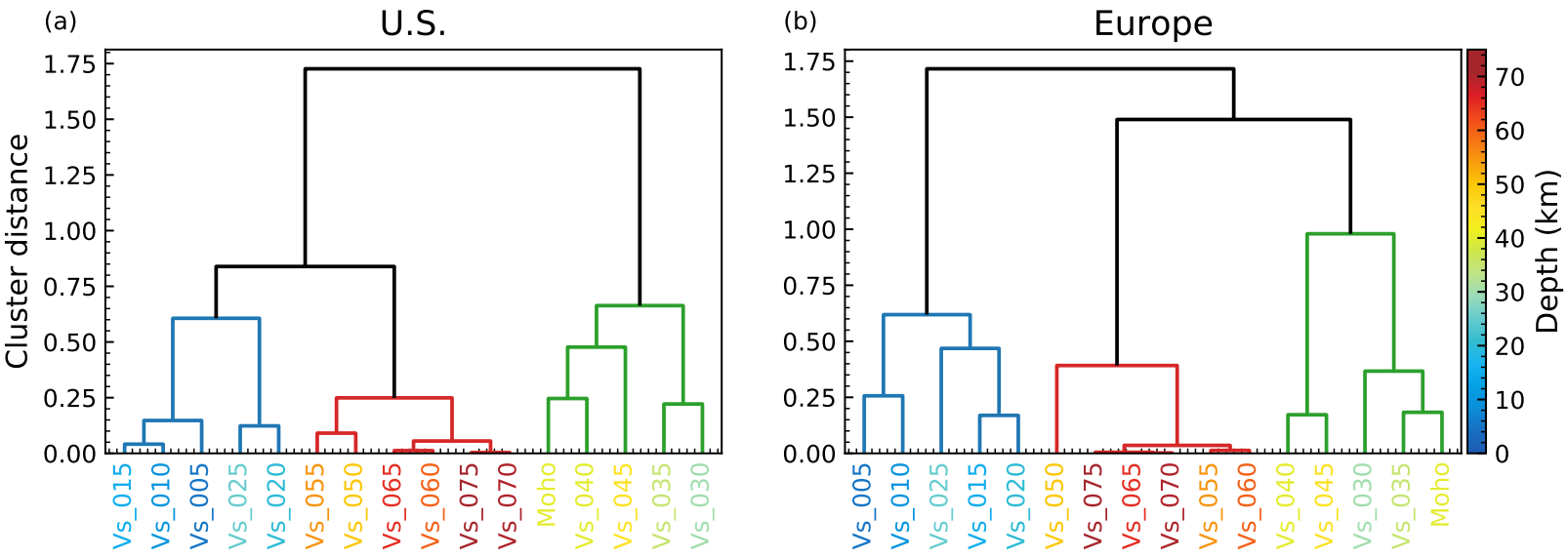

Figure 4: **Clustering of seismic structural variables.** Cluster analysis is performed to identify principal independent seismic structural variables and determine if they are the same in the US and Europe. (a) The arrangement (dendrogram) of seismic structural variables for the US based on hierarchical clustering (**section 2.2.2**). The seismic structural variables (x-labels) are color-coded by depth. For example, Vs_015 denotes shear wavespeed at 15 km depth. The distances between clusters (vertical axis) are measured based on Ward's method. (b) Similar to (a) but for European seismic variables. For both the US and European data, three variables (Vs_015, Vs_065, and Moho) represent the three clusters for the crust (blue), crust-mantle boundary (green), and uppermost mantle (red). These three variables, v, are part of the input to the Machine Learning models (**eq.** (1)).

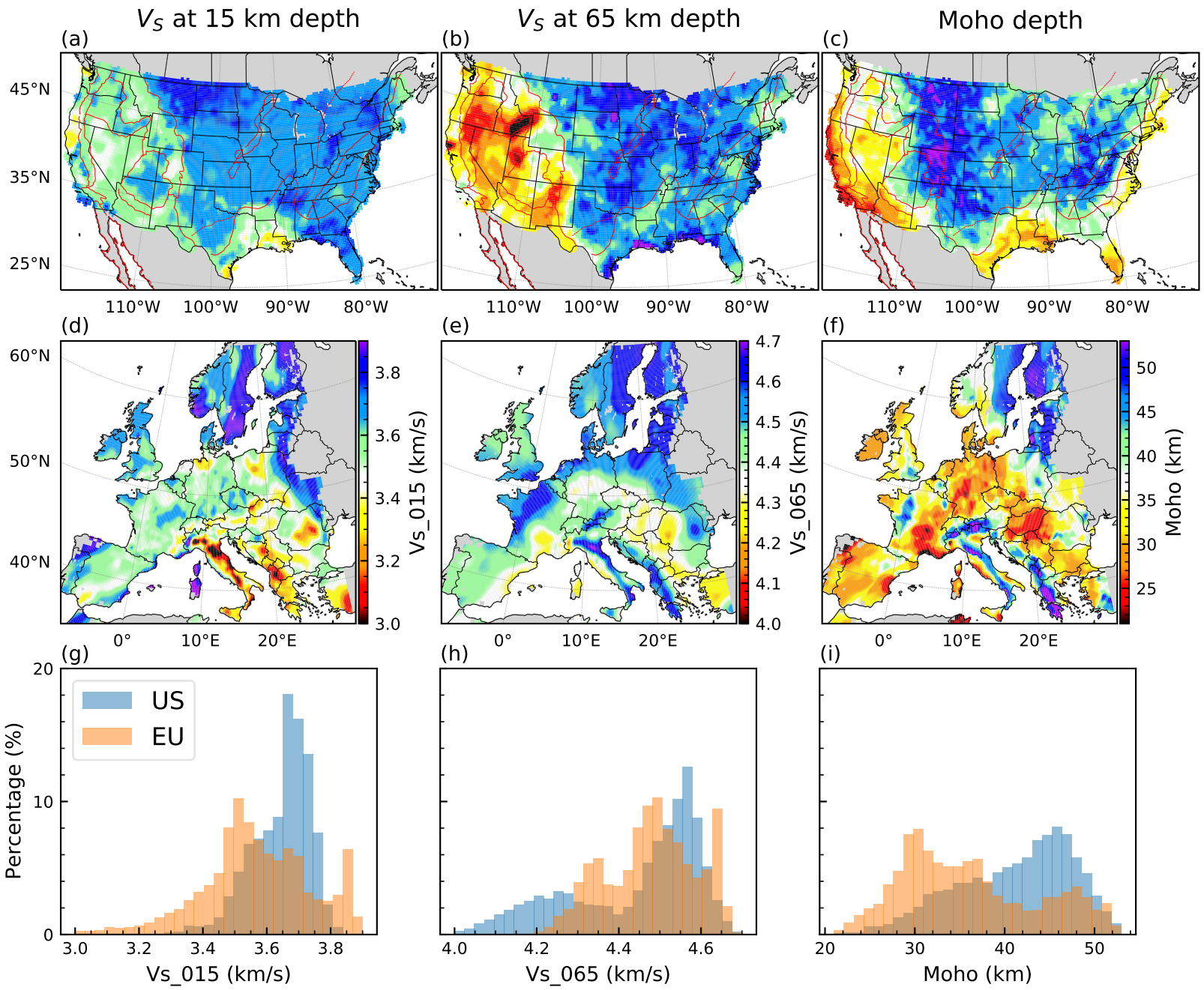

Figure 5: **Three representative seismic structural variables identified by the cluster analysis (Fig. 4).** (a)–(c) The US seismic structural variables from Shen and Ritzwoller [33]: (a) V_S at 15 km depth (Vs_015), (b) V_S at 65 km depth (Vs_065), and (c) Moho depth (Moho). (d)–(f) Similar to (a)–(c) except for the European seismic structure of Lu, Stehly, and Paul [34]. The seismic structure and heat flux (**Fig. 2**ad) are similar, particularly for (b) & (e), V_S at 65 km depth. (g)–(i) Histograms of (g) V_S at 15 km depth, (h) V_S at 65 km depth, and (i) Moho depth. The distributions are significantly different between the US and Europe .

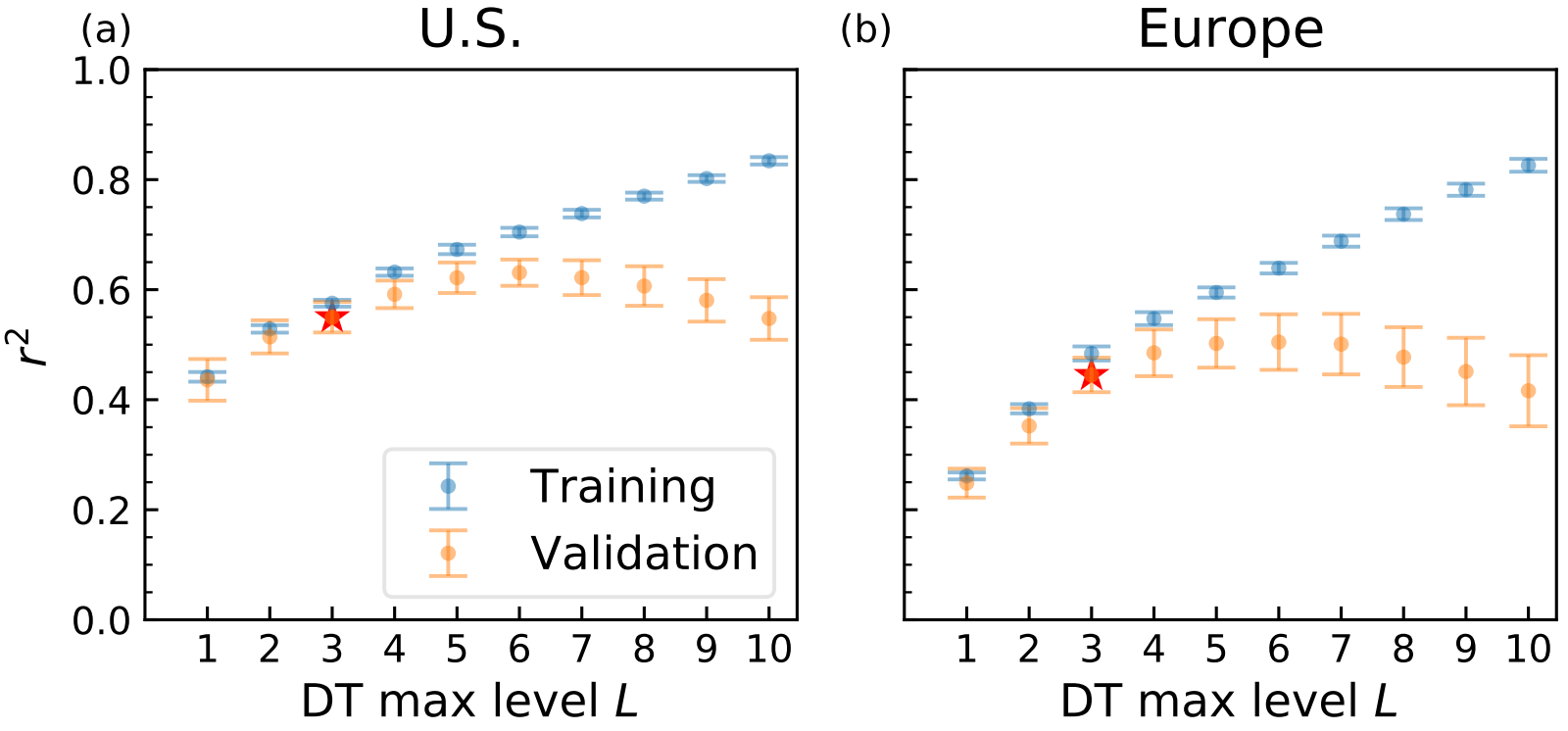

Figure 6: **Choosing the maximum level of the Decision Tree (DT) models.** (a) The r^2 (data misfit) is plotted as a function of maximum tree level L. The r^2 measures the proportion of observed heat flux variations predicted by the model (**eq.** (13)). Error bars denote mean $\pm$ standard deviation for the training (blue) and validation (orange) data in the US, respectively (**section 4.2**). The model is trained to fit the training data but not the validation data, so the training data are fit better. (b) Similar to (a) except for the European data, which are fit worse than the US data. This is part of the basis for our choice of $L = 3$ (star) as a trade-off between model accuracy (high r^2) and simplicity (low L).

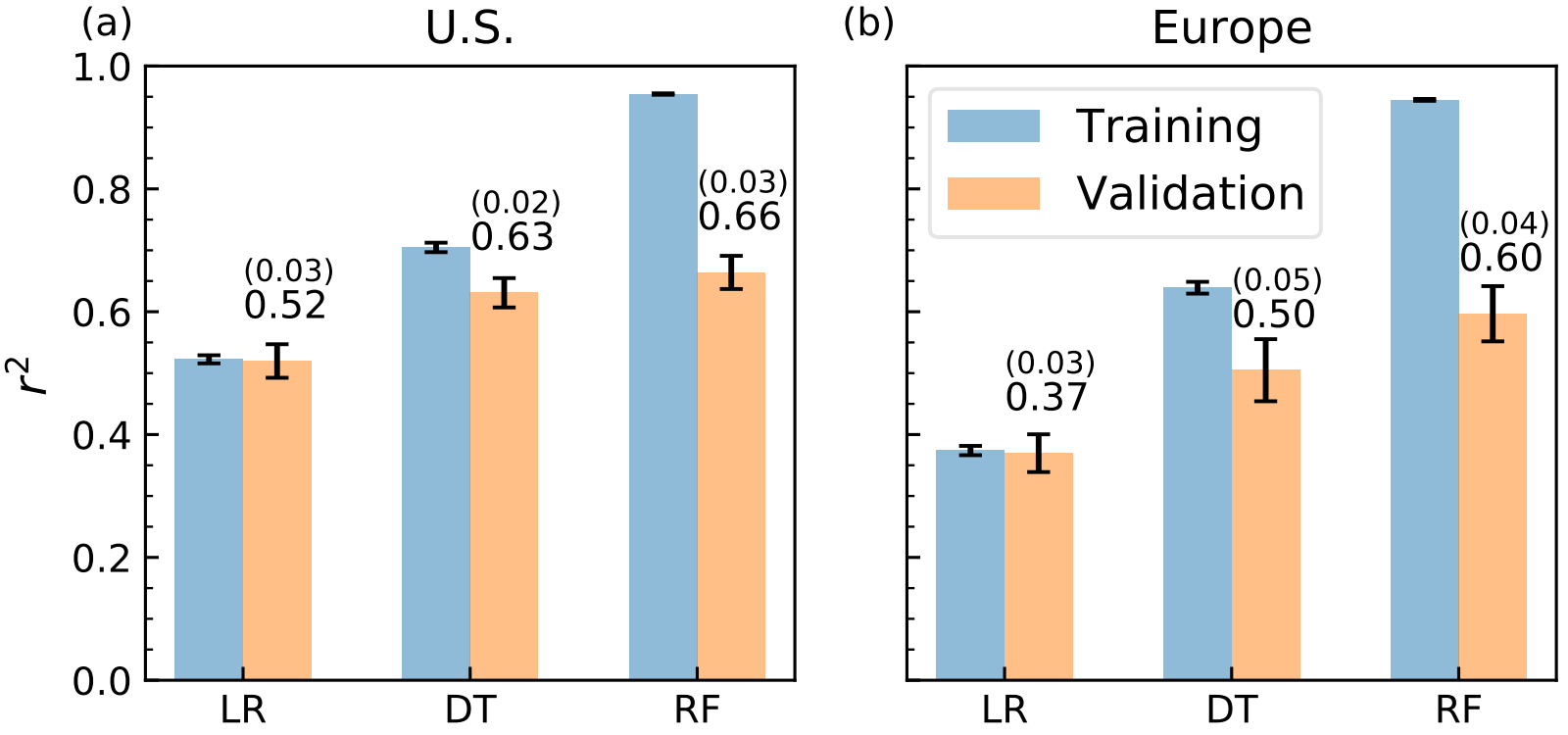

Figure 7: **Comparison of model accuracy based on validation within a continent.** (a) Based on the US data alone, the validation r^2 (orange), model applied to the test data, and associated training r^2 (blue) are shown for the Linear Regression (LR) model, the Decision Tree (DT) model ($L = 5$), and the Random Forest (RF) model (400 trees). The r^2 measures the proportion of observed heat flux variations predicted by each model (**eq.** (13)). Error bars denote mean ± standard deviations from 20-fold validation (**section 4.2**), and the numeric values are also annotated for the validation data (numbers in parentheses denote standard deviations). (b) Similar to (a) but for European data, which are fit worse than the US data. For both the US and European data, the Decision Tree and the Random Forest models fit the data similarly but are more accurate than the Linear Regression model.

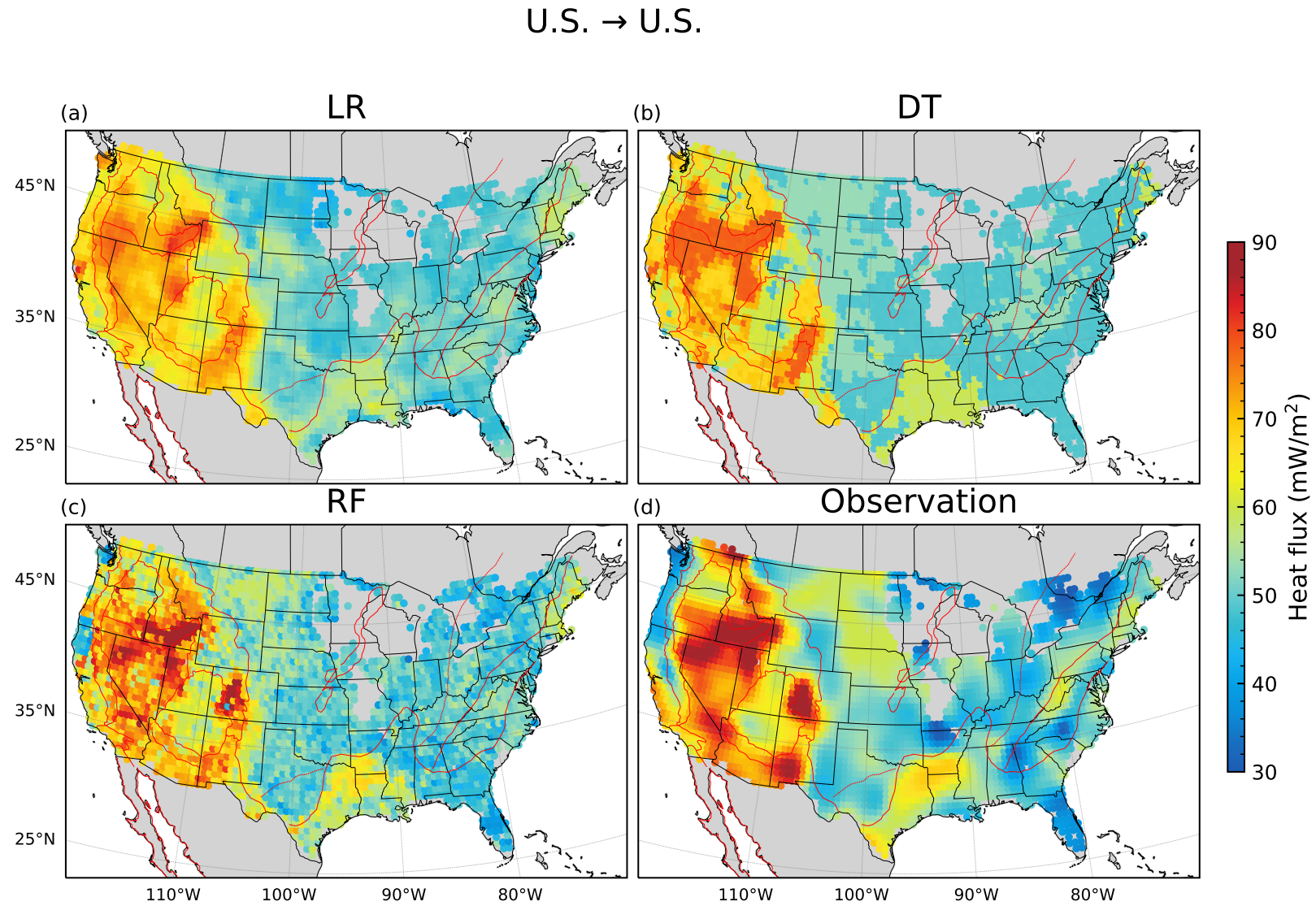

Figure 8: **Comparison of model accuracy based on validation with the US data alone.** (a) The Linear Regression (LR) model is trained with the training data and validated on the validation data. The predictions using the validation data are shown in (a), which should be compared with (d) observations (same as **Fig. 2**a). (b) & (c) Similar to (a) but for (b) the Decision Tree (DT) model ($L = 3$) and (c) the Random Forest (RF) model. The Linear Regression model predictions are the most smooth but least accurate, while the Random Forest model predictions are the most accurate but have noisy small scale variations. The Decision Tree model strikes a balance between accuracy and spatial resolution.

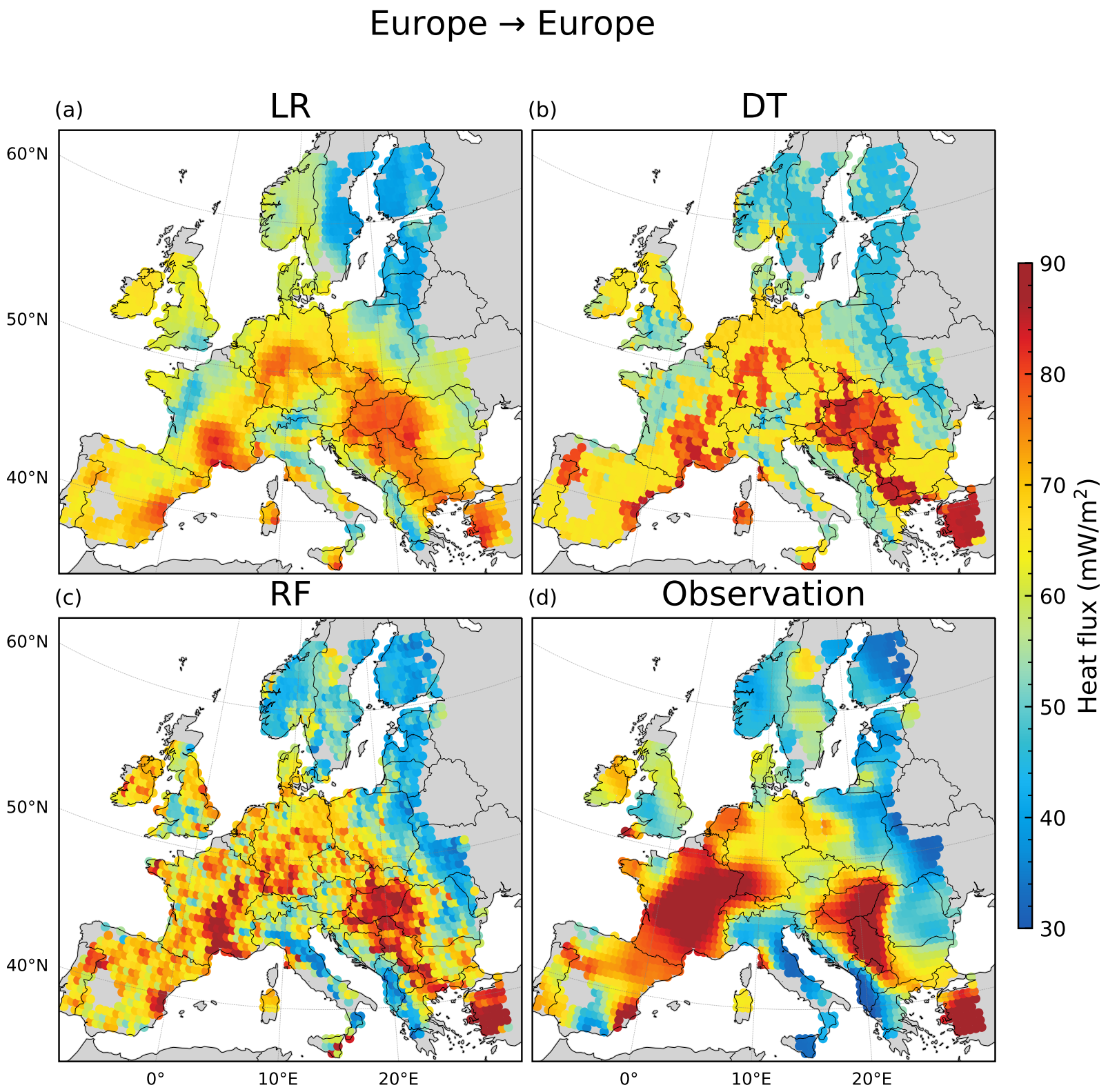

Figure 9: **Comparison of model accuracy based on validation with the European data alone.** Similar to **Fig. 8** but based on the European data alone. The relative accuracy and spatial resolution for different model predictions are similar to those using the US data alone, but the European predictions generally have larger differences with observations and are thus less accurate.

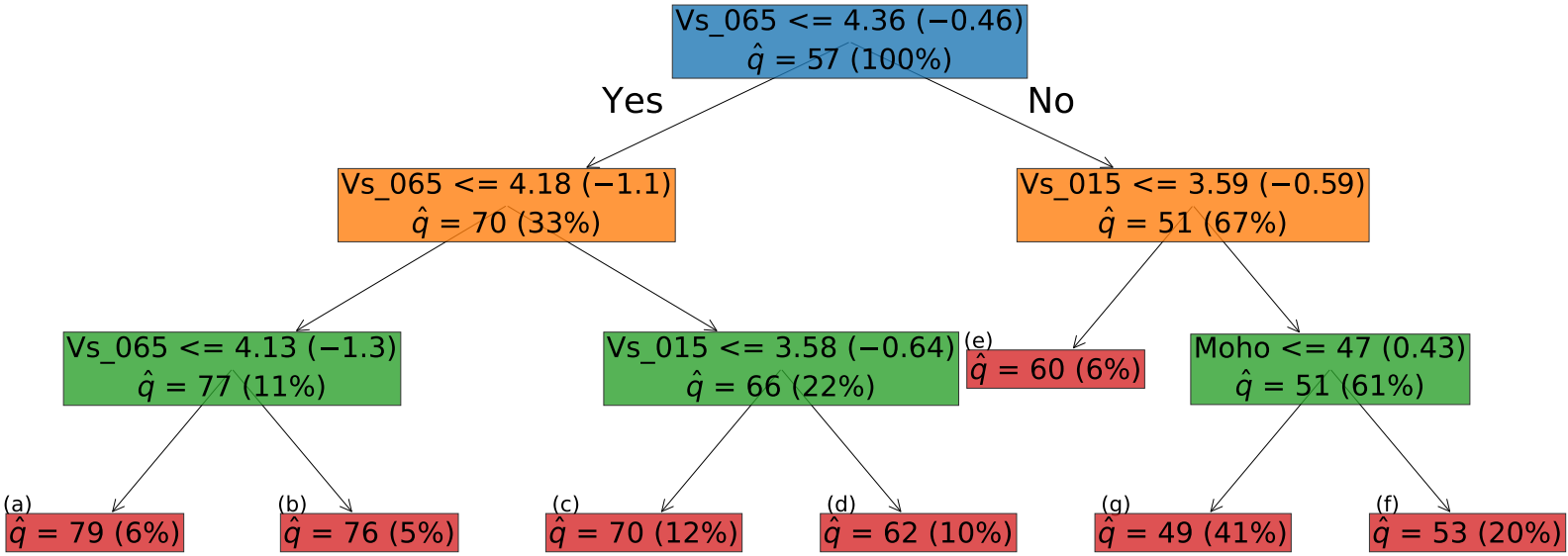

Figure 10: **The Decision Tree model trained using the US data alone.** The structure of the Decision Tree model trained using the US data alone, with a maximum level of three: $L = 3$. The nodes (boxes) are color-coded by level L, where blue, orange, and green denote $L = 1, 2, 3$, respectively, for the internal nodes, and the leaf nodes (terminal boxes) are color-coded in red. In the internal nodes, the first row shows the splitting criterion, $v \leq v_*$, where v and v_* denote the splitting variable and its threshold, respectively (**eq.** (10)). The unit is km for the Moho depth, and km/s for crustal and uppermost mantle V_S. The standardized threshold values are shown in parenthesis. The second row presents the predicted heat flux $\hat{q}$ and the percentage of the total data included in the prediction. The two arrows below an internal node represent a split of the parent data into two parts, where the left and right arrows denote the satisfaction ($v \leq v_*$) and violation ($v > v_*$) of the splitting criterion, respectively. In the seven leaf nodes, only the predicted heat flux $\hat{q}$ is shown. Each leaf node yields a decision rule and is identified with a letter label (a)–(g). These seven heat flux values (79, 76, 70, 62, 60, 53, 49 $\mathrm{mW/m^2}$) constitute the predicted map of heat flux (**Fig. 12**c). These decision rules are further illuminated in **Fig. 11**.

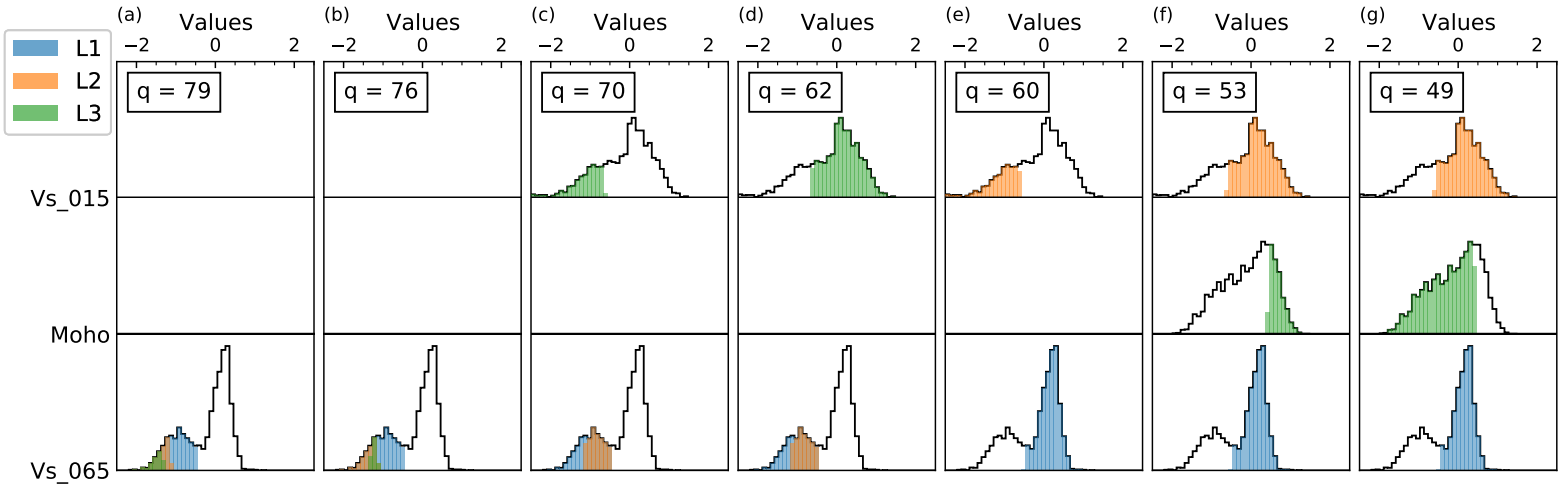

Figure 11: **Decision rules of the US-trained Decision Tree model in Fig. 10.** Each column denotes a decision rule (a unique path from the root node to one leaf node), ordered by decreasing heat flux predictions $\hat{q}$ from left to right. Each row represents one of the three seismic structural variables and the variables are increasing with depth from top to bottom. The statistical distributions of the variables are shown as black histograms. For each decision rule, the 3-D seismic variable space is successively split by the value ranges of each of the three variables, with the order of splitting color-coded in blue, orange, and green for $L = 1, 2, 3$ (**section 3.1.2**), which is consistent with the node colors in **Fig. 10**. Note that the distributions are often split at valleys or peaks, which tend to correlate with geological boundaries.

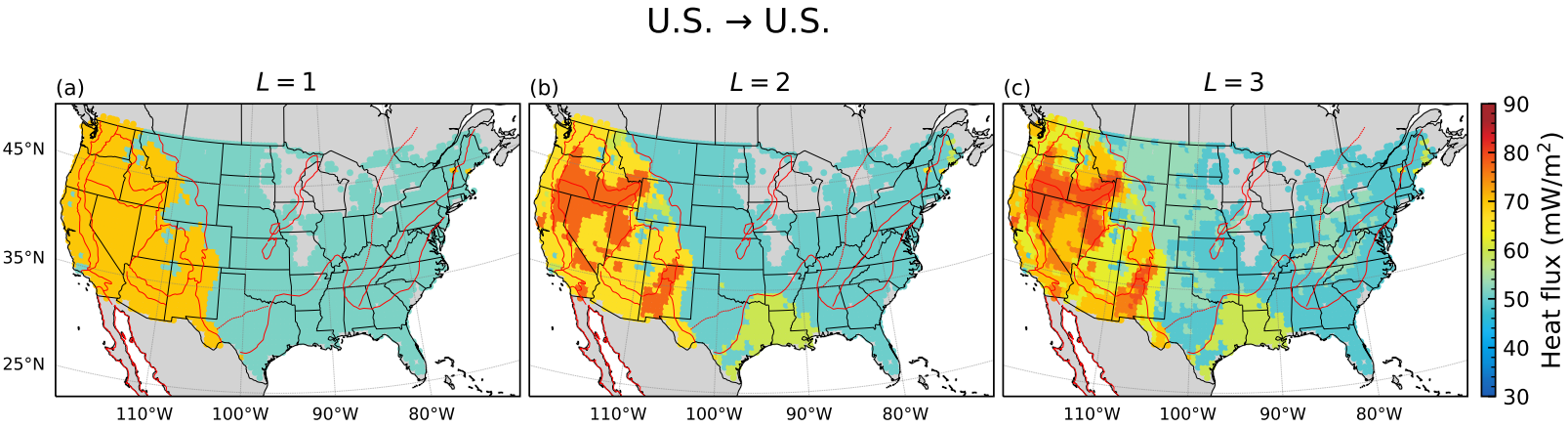

Figure 12: **Increasing complexity of the Decision Tree models as the number of levels (L) is increased.** Heat flux predictions are plotted for Decision Tree models with maximum levels of (a) 1, (b) 2, and (c) 3. The unique advantage of the Decision Tree model is that increased complexity with levels tends to split the whole area into regions corresponding with geological provinces (despite no such geographical information given), and it can yield a specific relationship between heat flux and seismic structure for each region.

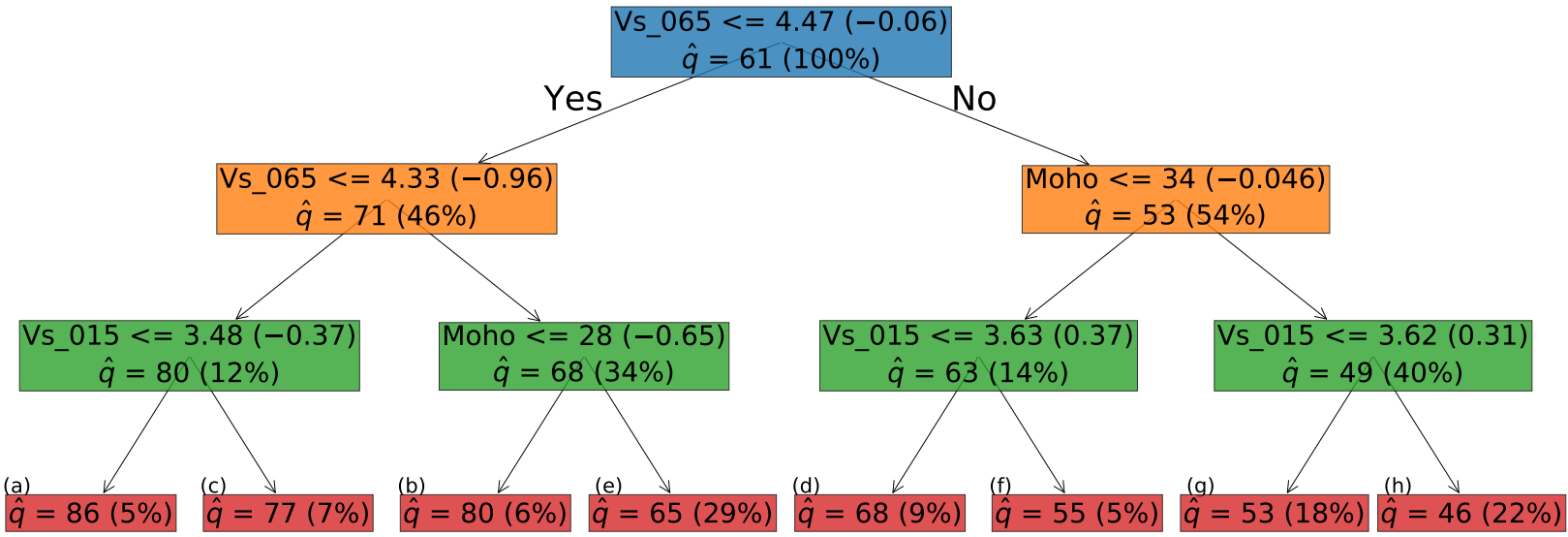

Figure 13: **Decision tree model trained using the European data alone.** Similar to **Fig. 10** except that the heat flux data and seismic structural information are from Europe. The deicsion rules (labeled (a)–(h)) are illustrated in **Fig. 14**.

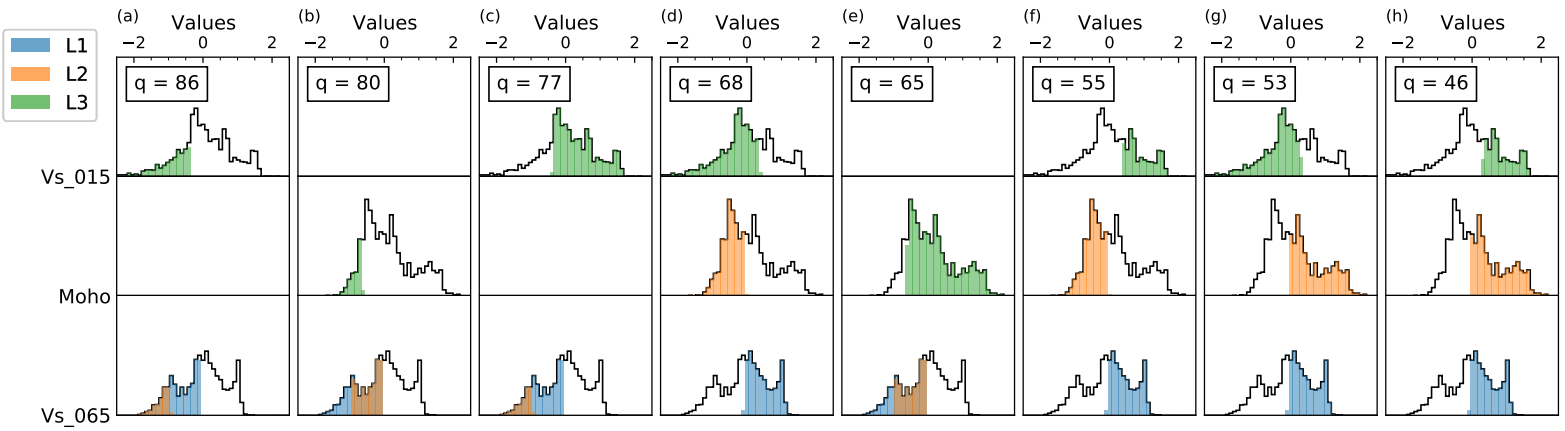

Figure 14: **Decision rules of the Europe-trained Decision Tree model in Fig. 13.** Similar to **Fig. 11** except for the European data alone. Note that the Moho depth plays a more important role than in the US-trained Decision Tree model (**Fig. 11**).

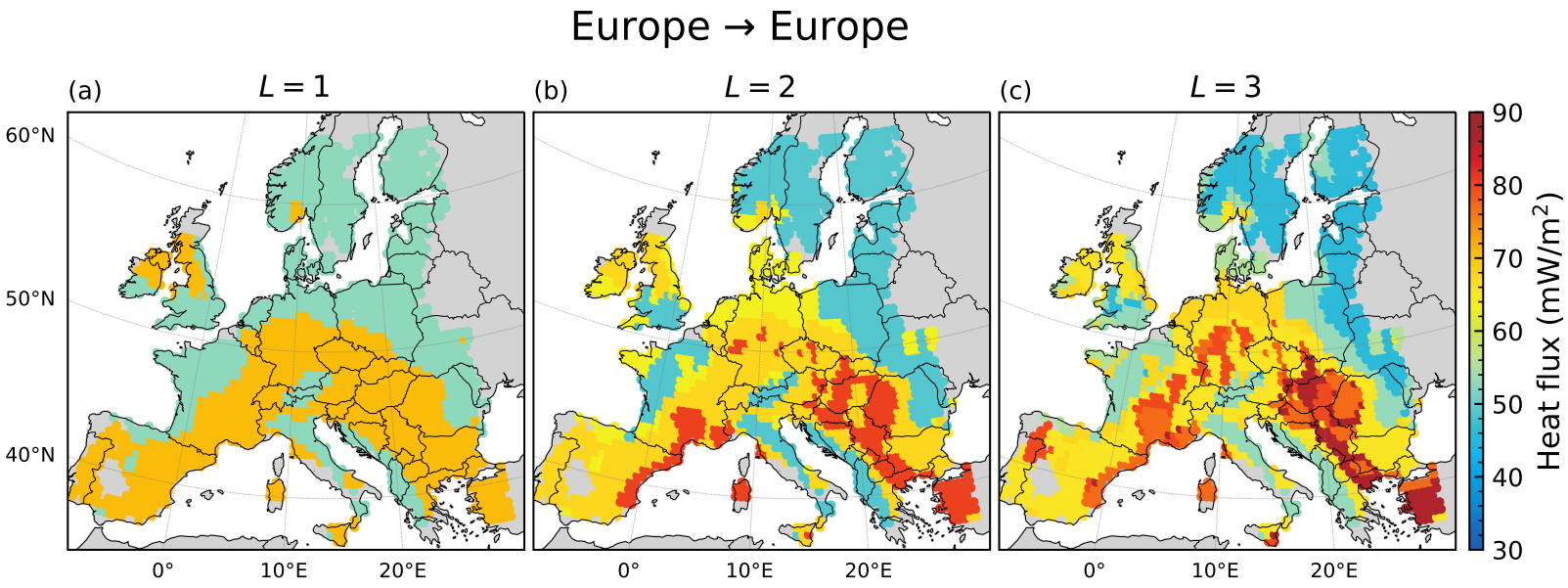

Figure 15: **Increasing complexity of the Decision Tree models as the number of levels (L) is increased using the European data alone.** This figure is similar to **Fig. 12** except for the European data. This figure should be compared with observations in **Fig. 2**d, and applying the US-trained models in **Fig. 20**. Note that geologically relevant provinces are successively identified by growing the tree.

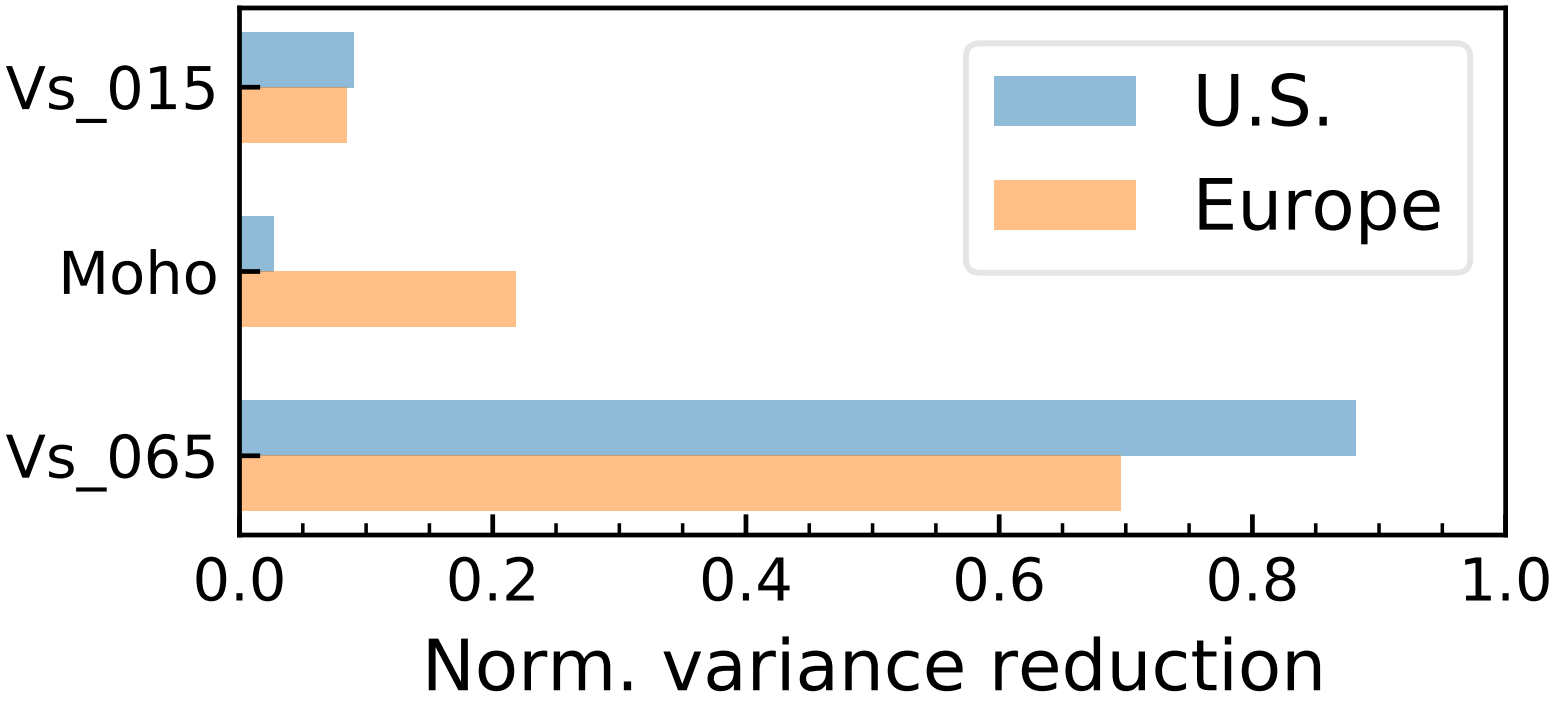

Figure 16: **Importance of seismic structural variables from the Decision Tree (DT) models.** Normalized variance reduction (Gini importance) is shown for the Decision Tree models based on the US data alone (blue; **Fig. 10**) and the European data alone (orange; **Fig. 13**). Uppermost mantle V_S is the most important and the Moho depth is more important for the European data than the US data. These findings agree with the Linear Regression coefficients (**Fig. S3**).

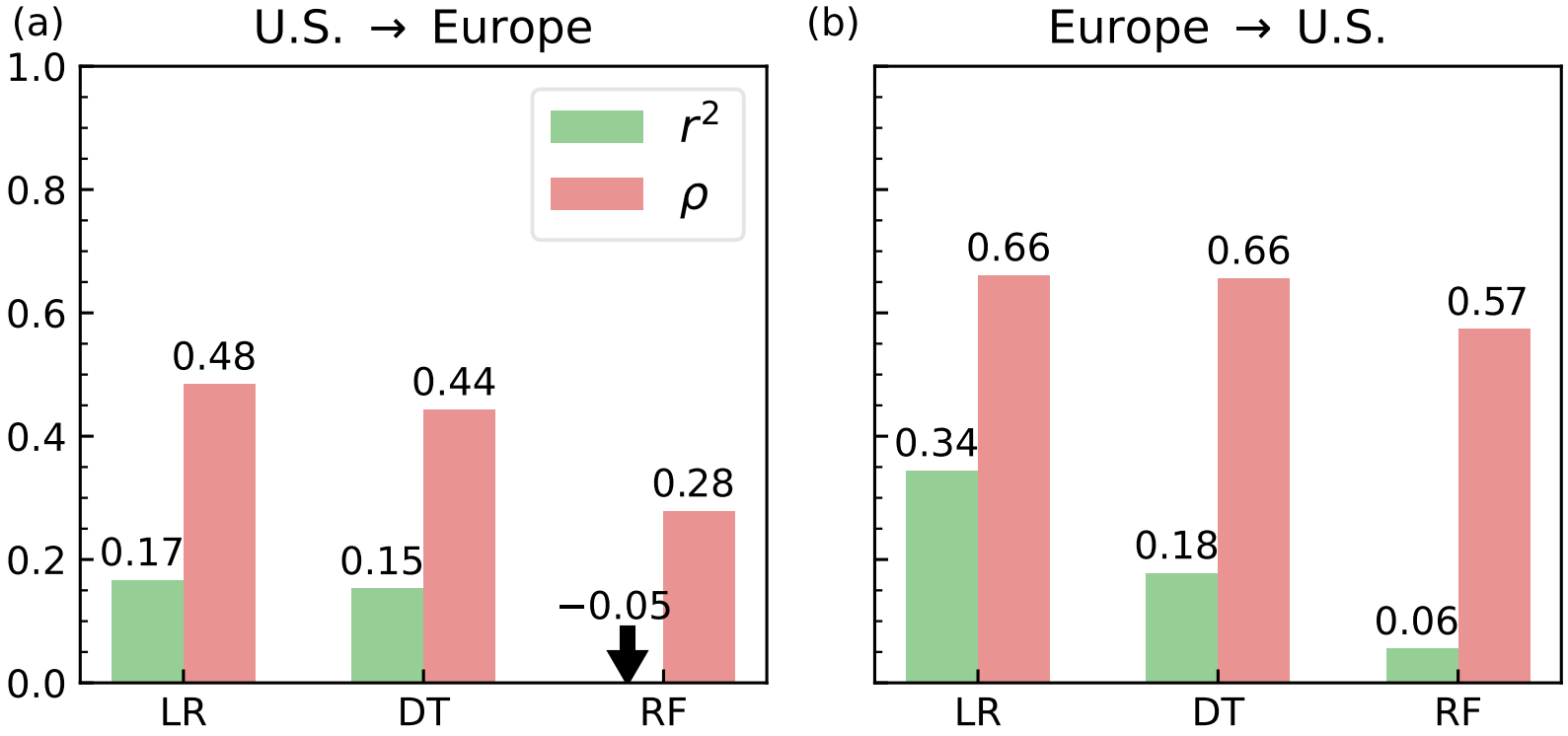

Figure 17: **Comparison of model transportability by cross-validation between the US and European data.** (a) The r^2 (overall misfit, **eq.** (13)) and ρ (geographical coherence, **eq.** (14)) are shown, applying the US-trained models to the European data. The r^2 of the Random Forest (RF) model is negative, i.e., worse than using the average European heat flux as a constant predictor. The Linear Regression and Decision Tree models are comparable and significantly more transportable than the Random Forest model. (b) Similar to (a) but for applying the Europe-trained models to the US data. The relative performance between the models is similar to applying the US-trained models to the European data.

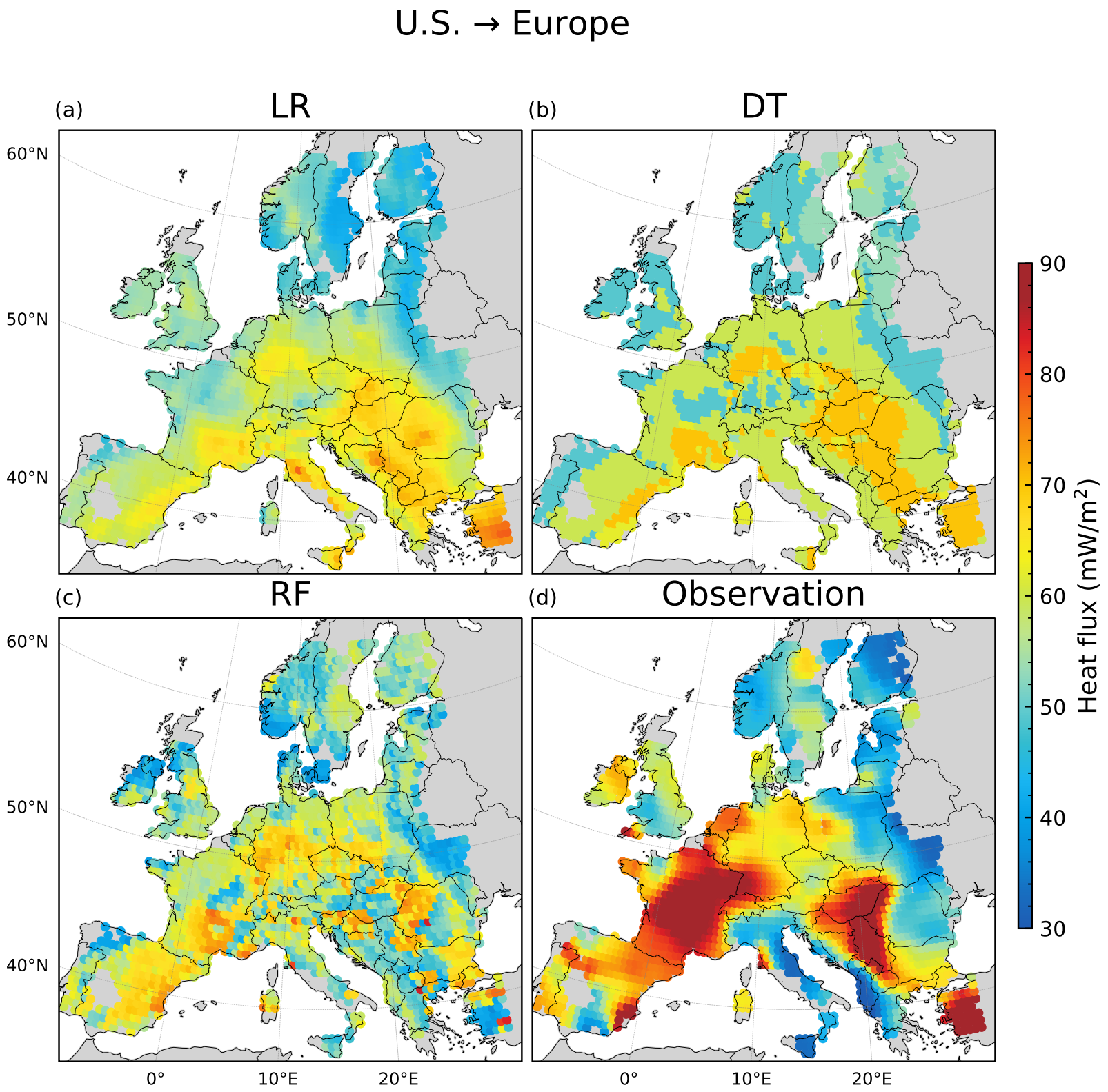

Figure 18: **Comparison of model transportability by applying the US-trained models to European data.** Similar to **Fig. 9**, except the models are trained with the US data. This figure should be contrasted with the predictions of the Europe-trained models on the European data in **Fig. 9**. The geographic patterns of heat flux are reasonably reproduced, but the absolute amplitudes are not.

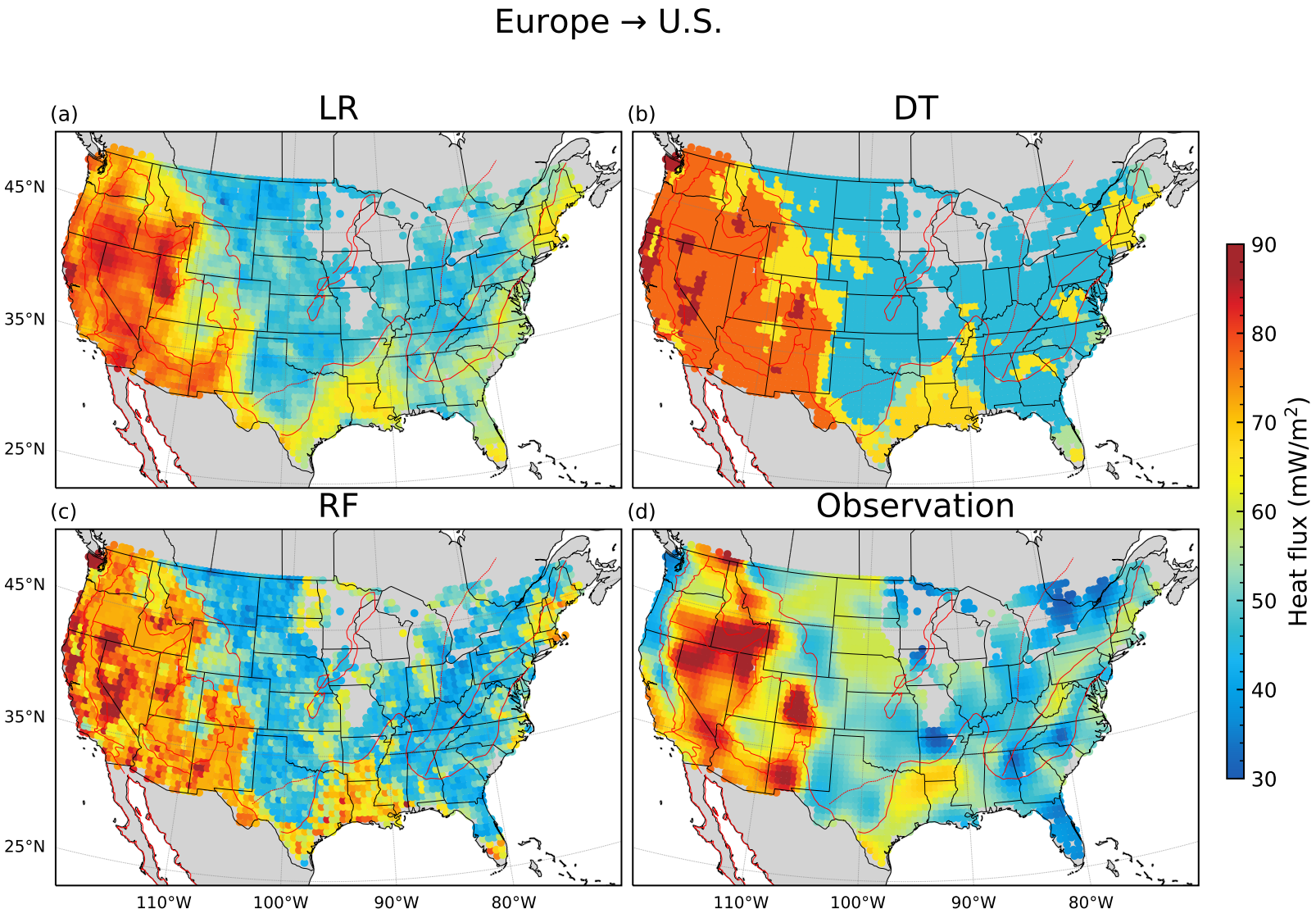

Figure 19: **Comparison of model transportability by applying the Europe-trained models to the US data.** Similar to **Fig.** 8, except the models are trained with the European data. This should be contrasted with the predictions of the US-trained models on the US data in **Fig.** 8. The geographic patterns of heat flux are reproduced better than the absolute amplitudes, both are better reproduced than applying the US-trained models to Europe (**Fig.** 18).

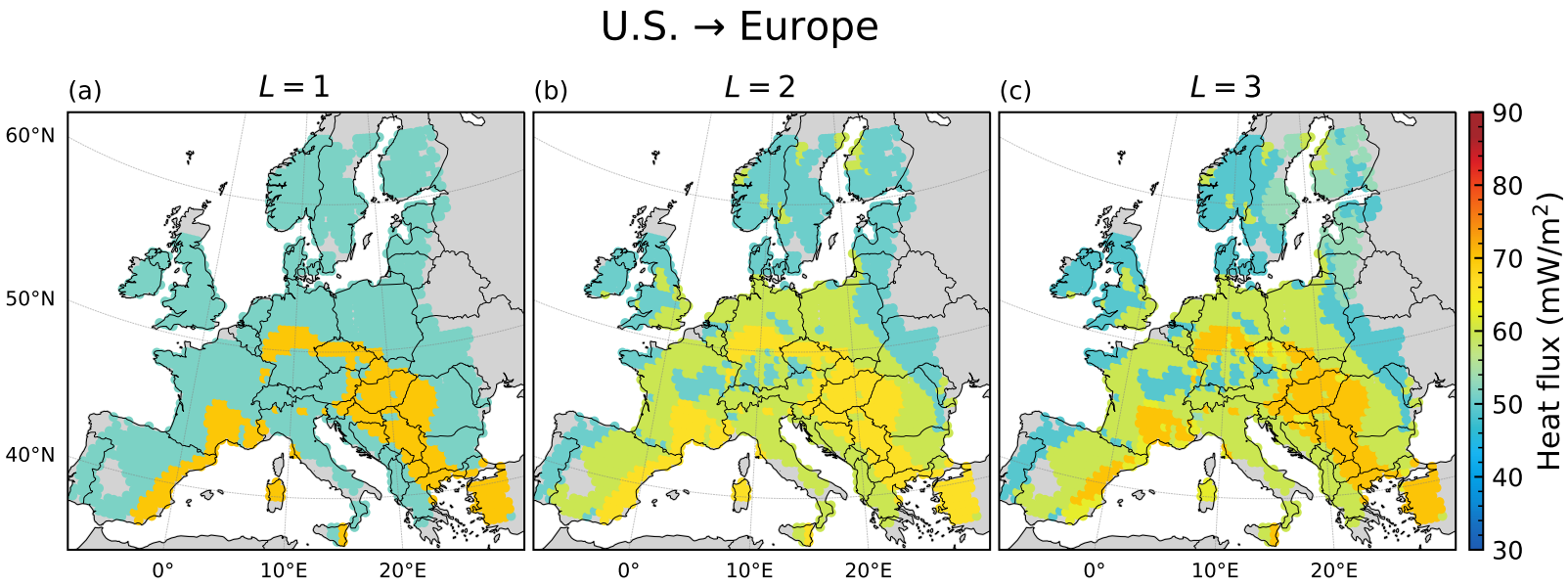

Figure 20: **Transporting the US-trained Decision Tree models to the European data.** This figure is similar to **Fig. 12**, but the models are trained with the US data (**Fig. 10**). This should be contrasted with the predictions of the Decision Tree models trained from the European data (**Fig. 15**). The geographic patterns of heat flux are better reproduced with increasing the level L, but the absolute amplitudes are under-predicted.

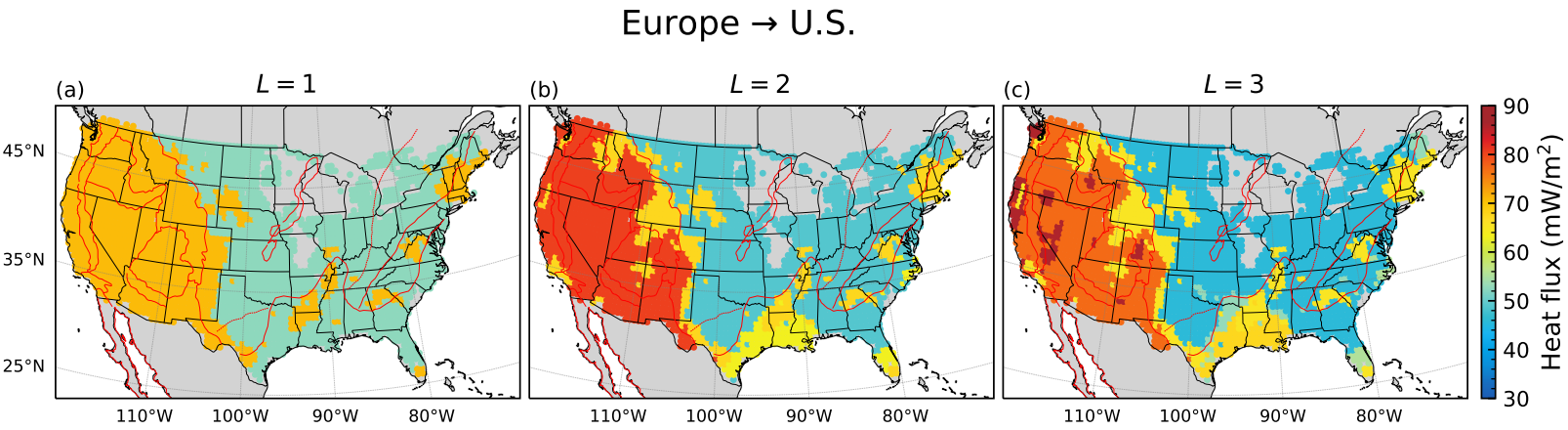

Figure 21: **Transporting the Europe-trained Decision Tree models to the US data.** Similar to **Fig. 20** but the models are trained with the European data (**Fig. 13**). The geographical patterns are similar to the predictions from the US-trained Decision Tree models, but the absolute amplitudes are over-predicted (**Fig. 12**).

Supplement

List of Supplementary Figures

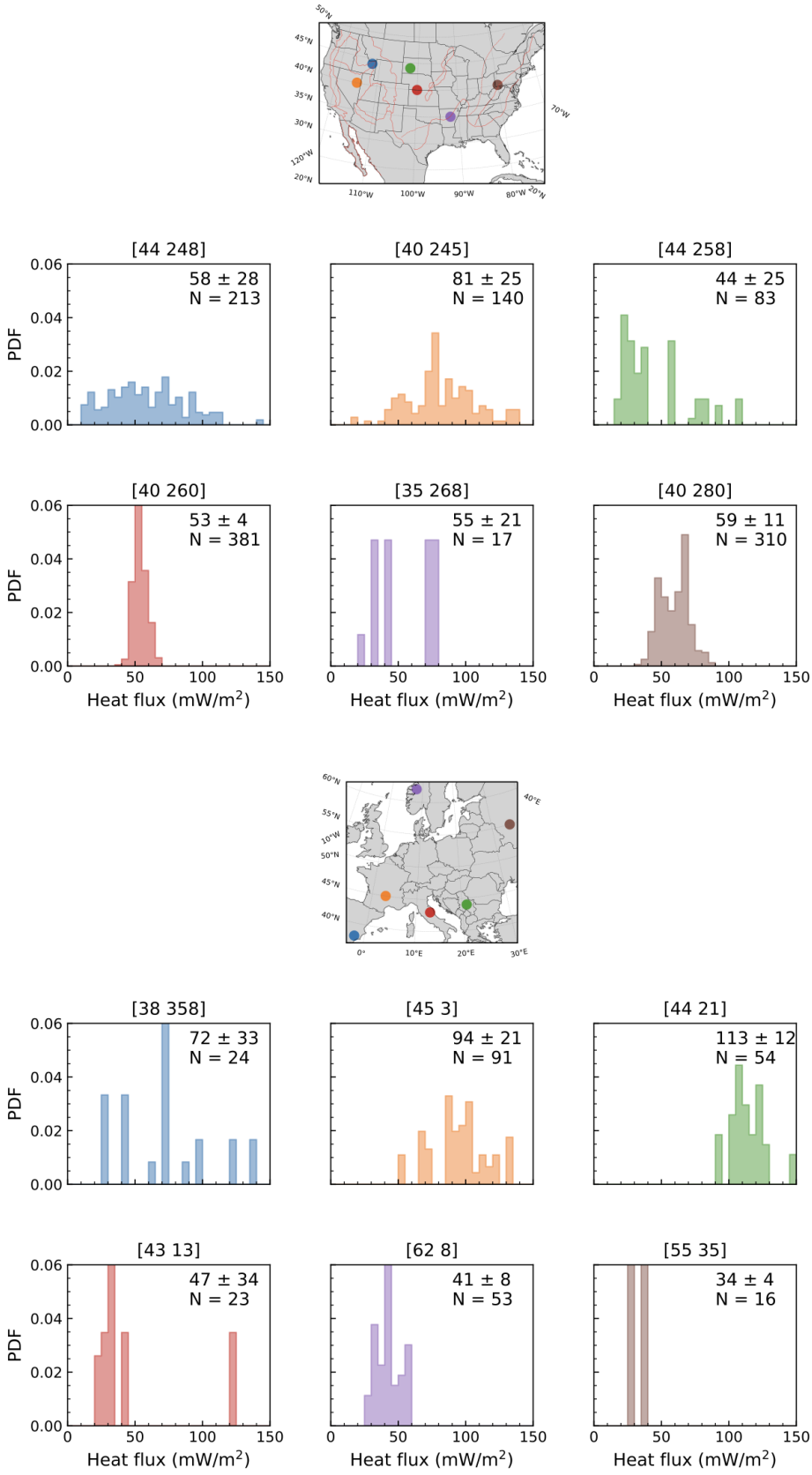

Figure S1: **Local distribution of heat flux observations.**

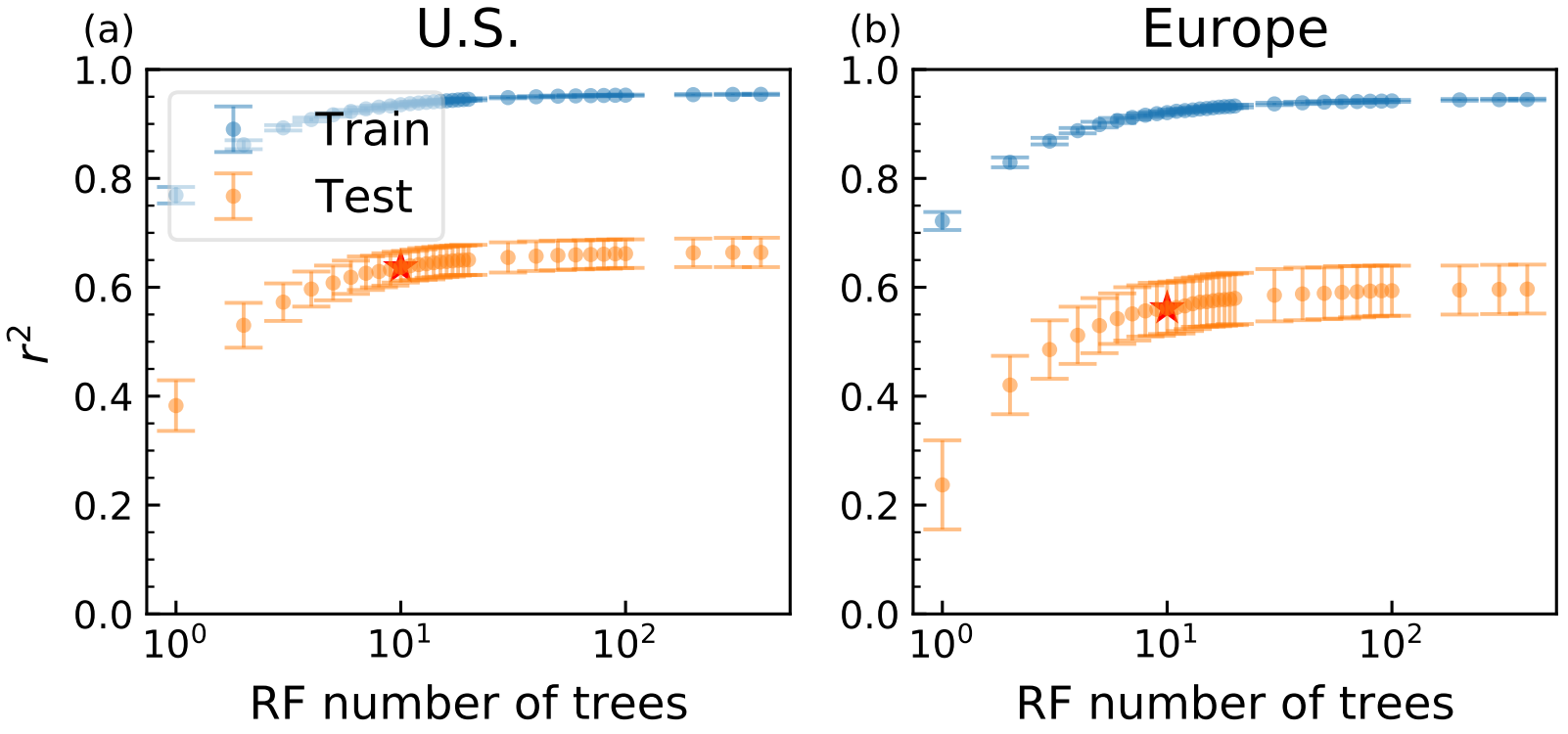

Figure S2: **Validation of the Random Forest (RF) models.** Similar to **Fig. 6** except for the Random Forest models. Note that the x scale is logarithmic.

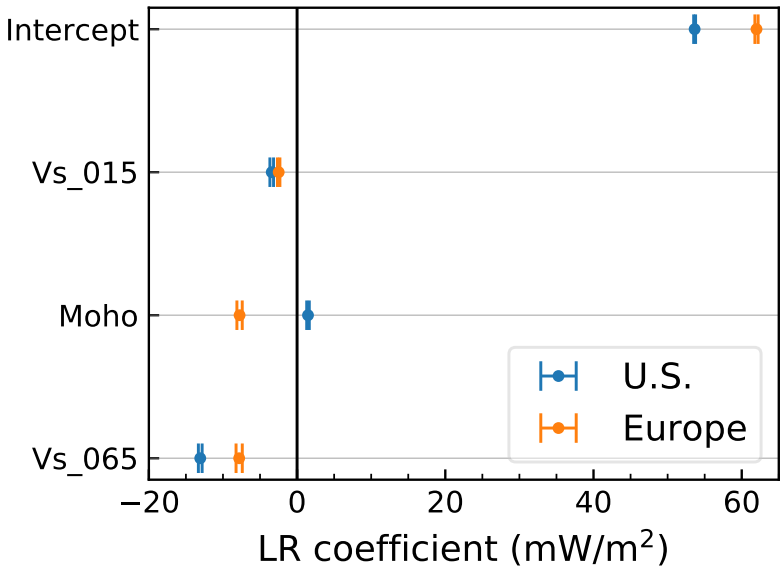

Figure S3: **Coefficients from the Linear Regression (LR) models.** Error bars denote the mean ± standard deviation of the coefficient values from the 20-fold validation (**section 3.2.1**), for the US (blue) and European (orange) data, respectively. Note that the background value (intercept) is systematically higher for the European data than the US data, and that the Moho depth has opposite effects between the two continents.

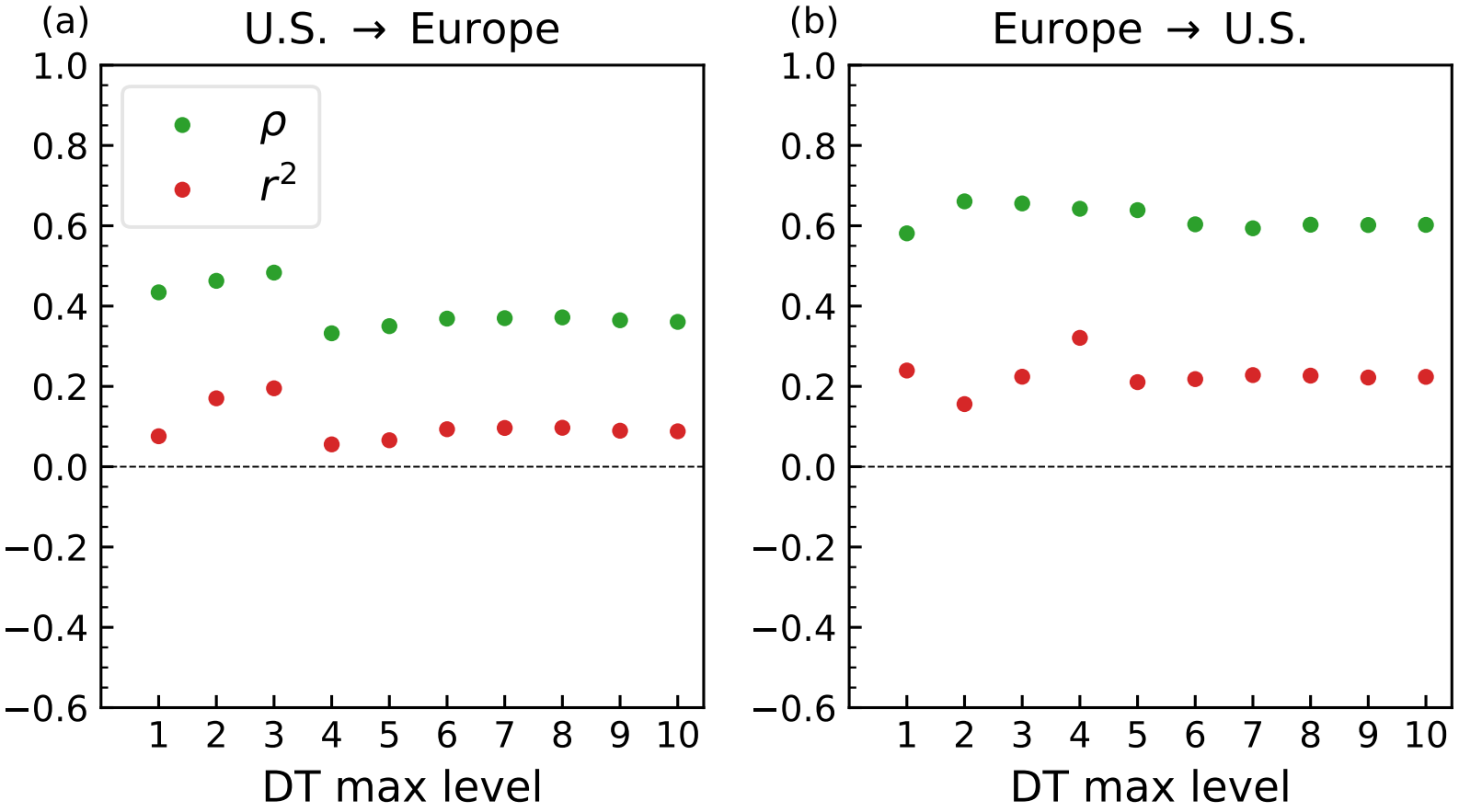

Figure S4: **Variation of transportability with the max level of the Decision Tree (DT) models.** The ρ and r^2 are plotted as a function of the Decision Tree max level, (a) from applying US-trained models to Europe, and (b) vice versa. Note the dip at $L = 3$ in (a). This figure should be compared with validation within a continent (**Fig. 6**).

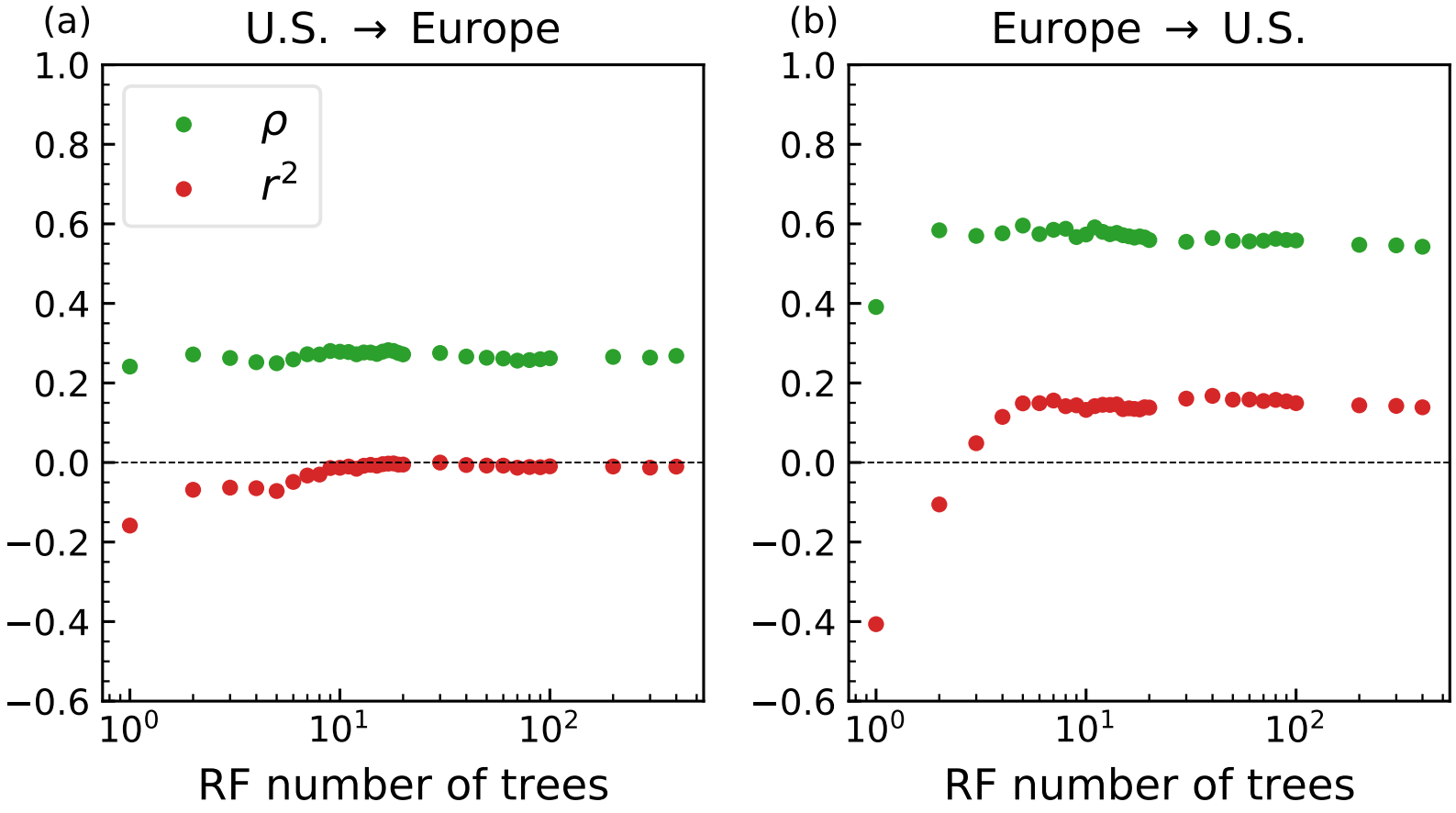

Figure S5: **Variation of transportability with the number of trees in the Random Forest (RF) models.** Similar to **Fig.** S4 except for the Random Forest models. This figure should be compared with validation within a continent (**Fig.** S2).

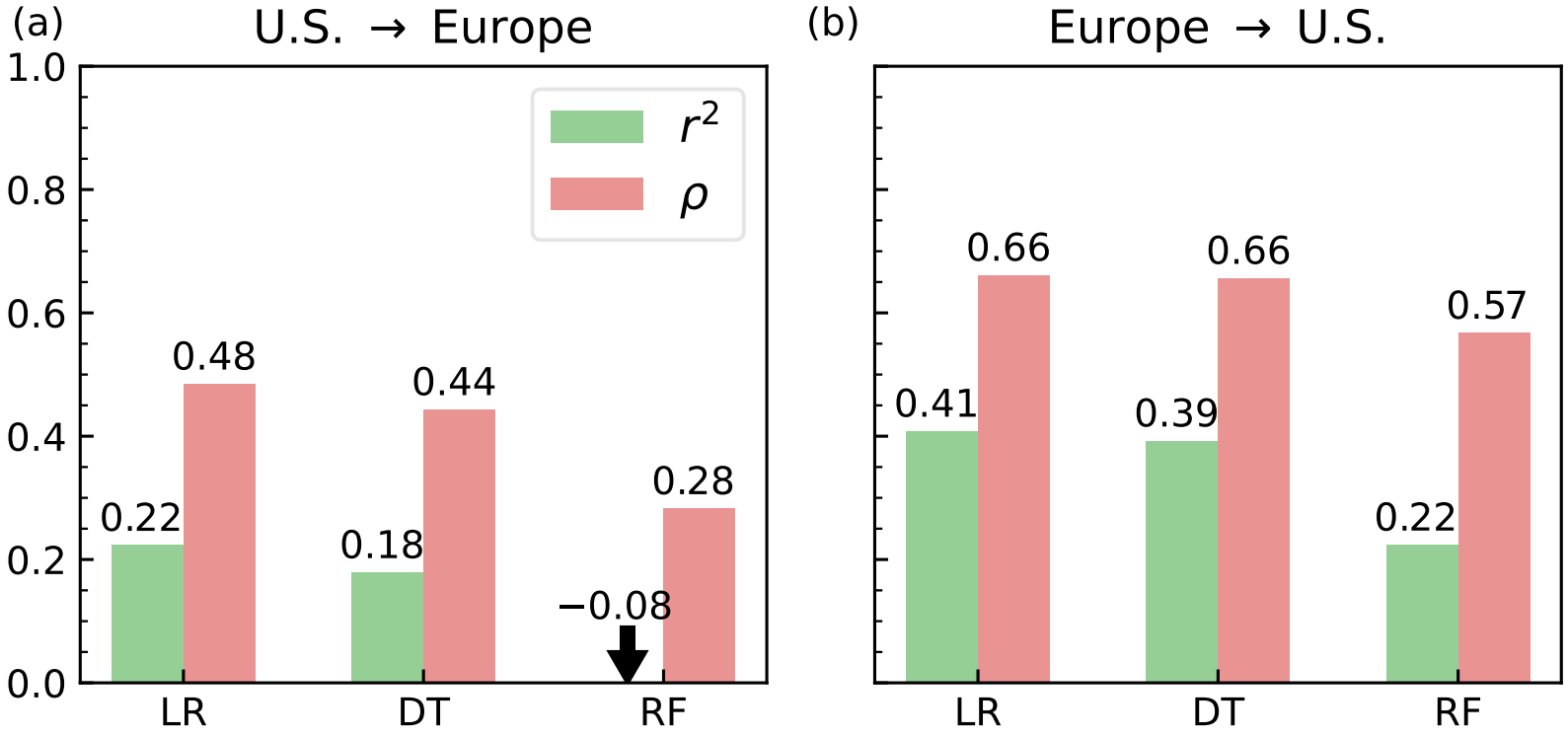

Figure S6: **Comparison of model transportability after standardizing heat flux.** Similar to **Fig. 17** but heat flux observations are standardized separately for both the US and Europe. Compared to using heat flux without standardization (**Fig. 17**), the geographical coherence ρ does not change, but the overall misfit r^2 is smaller and the absolute amplitudes are better predicted.